Materials Today Bio 26 (2024) 101113

Contents lists available at ScienceDirect

Materials Today Bio

journal homepage: www.journals.elsevier.com/materials-today-bio

Natural blackcurrant extract contained gelatin hydrogel with photothermal and antioxidant properties for infected burn wound healing

Yachao Yu [a], Mengyu Yang [a], Hua Zhao [a], Chen Zhang [a], Kaiyue Liu [a], Jingmei Liu [a], Chenghao Li [a], Bingjie Cai [b,***], Fangxia Guan [a,**], Minghao Yao [a,*]

[a] School of Life Science, Zhengzhou University, 100 Science Road, Zhengzhou, 450001, China
[b] Department of Dermatology, the First Affiliated Hospital of Zhengzhou University, Zhengzhou, China

A B S T R A C T

Burns represent a prevalent global health concern and are particularly susceptible to bacterial infections. Severe infections may lead to serious complications, posing a life-threatening risk. Near-infrared (NIR)-assisted photothermal antibacterial combined with antioxidant hydrogel has shown significant potential in the healing of infected wounds. However, existing photothermal agents are typically metal-based, complicated to synthesize, or pose biosafety hazards. In this study, we utilized plant-derived blackcurrant extract (B) as a natural source for both photothermal and antioxidant properties. By incorporating B into a G-O hydrogel crosslinked through Schiff base reaction between gelatin (G) and oxidized pullulan (O), the resulting G-*O*-B hydrogel exhibited good injectability and biocompatibility along with robust photothermal and antioxidant activities. Upon NIR irradiation, the controlled temperature (around 45–50 °C) generated by the G-*O*-B hydrogel resulted in rapid (10 min) and efficient killing of *Staphylococcus aureus* (99 %), *Escherichia coli* (98 %), and *Pseudomonas aeruginosa* (82 %). Furthermore, the G-*O*-$B_{0.5}$ hydrogel containing 0.5 % blackcurrant extract promoted collagen deposition, angiogenesis, and accelerated burn wound closure conclusively, demonstrating that this well-designed and extract-contained hydrogel dressing holds immense potential for enhancing the healing process of bacterial-infected burn wounds.

1. Introduction

Full-thickness burns, known as one of the most challenging wounds to treat, can cause extensive damage to the epidermis, dermis, and even subcutaneous tissues [1]. Due to the destruction of the skin's structure and elasticity, these types of burns often result in fragile and easily ruptured wounds [2,3]. The disruption of the skin's protective barrier renders the wound susceptible to bacterial and other microbial infections. These infections can result in further deterioration, delayed healing, heightened pain, and additional complications [4–6]. Currently, various clinical strategies are employed to treat burn wound infections, including antibiotic treatment [7–9], surgical interventions [10], photothermal therapy [11], as well as the use of wound dressings and coverings. While antibiotic treatment is necessary in certain cases, it is essential to consider its drawbacks and limitations [12]. These may include issues with drug resistance, side effects associated with systemic antibiotics, and allergic reactions. Photothermal therapy (PTT) is a method that utilizes photothermal technology to inhibit microbial growth [13]. This approach harnesses the ability of photosensitizers to convert light energy into heat energy, thereby destroying the cellular structure and metabolic function of microorganisms. PTT offers several advantages over other antibacterial methods, including efficient sterilization, absence of chemical residues, spatio-temporal controllability, and the ability to simultaneously target multiple microorganisms [14–16]. However, it is important to note that current photosensitizers still have some limitations, such as the propensity for phototoxic reactions, poor selectivity towards light, and the employment of relatively complex and costly components [17,18]. These factors may compromise treatment efficacy or lead to unnecessary side effects. In addition, oxidative stress and inflammatory response at the wound site cannot be ignored [19,20]. Thus, there is a demand for the development of natural, low-toxicity, straightforward, and cost-effective photosensitizers and antioxidant materials.

Hydrogel is commonly used in burn wound dressings due to its ability to keep the wound moist, absorb exudate, prevent bacterial infection, and provide protection [21–24]. Gelatin, a natural protein, is often used to prepare hydrogel due to its biocompatibility, gel-forming ability, and drug-delivery capability [25,26]. Additionally, gelatin-based hydrogels offer an appropriate structure and moisture for wound dressing, prolongs the drug effect, enhances efficacy, and

* Corresponding author.
** Corresponding author.
*** Corresponding author.
E-mail addresses: 112064777@qq.com (B. Cai), guanfangxia@126.com (F. Guan), yao453343550@126.com (M. Yao).

https://doi.org/10.1016/j.mtbio.2024.101113
Received 14 March 2024; Received in revised form 31 May 2024; Accepted 3 June 2024
Available online 3 June 2024

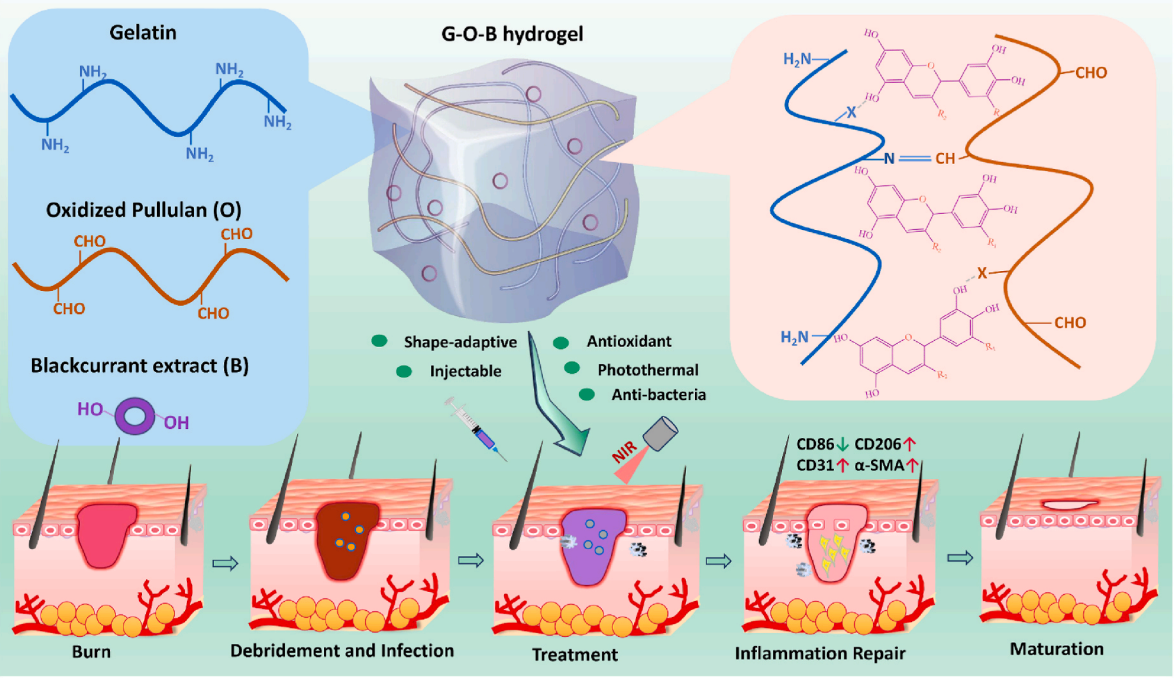

Scheme 1. The preparation, crosslinking mechanism, and pro-healing mechanism of multifunctional gelatin-oxidied pullulan hydrogel-blackcurrant extract (G-*O*-B) on bacterial-infected burn wounds.

facilitates wound healing [27–29]. Pullulan, a natural polysaccharide produced by fungal fermentation, is non-toxic, non-irritating, and biocompatible, aligning with the concept of green and sustainable development [30,31]. Blackcurrant extract, derived from black currant, is rich in active ingredients such as anthocyanins, which has strong antioxidant activity and protects cells from free radical damage [32,33]. It has also been reported to enhance immune system function and reduce the risk of infections and chronic diseases [34]. Despite their potential photothermal conversion, antioxidant, and antimicrobial properties, the utilization of natural plant extracts in burn wounds remains relatively unexplored. Moreover, the synergistic effect of these extracts combined with hydrogel dressings on wound healing requires further investigation.

Herein, the gelatin (G) and oxidized pullulan (O) were cross-linked by Schiff base reaction to prepare G-O hydrogel, and then the plant-derived blackcurrant extract (B) was loaded into the G-O hydrogel through intermolecular hydrogen bonding with G/O and act as a photothermal agent and antioxidant to prepare G-*O*-B hydrogel for promoting the healing of infectious burn wounds (Scheme 1). The obtained G-*O*-B hydrogel possesses good injectable, shape-adaptive, photothermal, antibacterial, antioxidant, and biocompatible properties, which are conducive to the healing of infected burn wounds.

2. Materials and methods

2.1. Materials

Gelatin was purchased from Sigma Aldrich Co., Ltd. (St. Louis, USA). Sodium periodate and pullulan were purchased from Aladdin Biochemical Technology Co., Ltd. (Shanghai, China). Blackcurrant extract (main specification of anthocyanin 5%–25 %) was bought from Jianfeng Natural Products Research and Development Co., Ltd. (Tianjin, China). The CCK8 kit was obtained from Everbright Holdings (USA). The live/dead fluorescence assay kit (Calcein AM/PI), safranine O, ABTS (2,2′- diazo bis (3-ethylbenzothiazoline 6-sulfonic acid), glutamate pyruvate transaminase (GPT) assay kit, glutamate oxaloacetate transaminase (GOT) assay kit, and tissue and blood alkaline phosphatase (AKP) assay kit were purchased from Solar Biotechnology Co., Ltd. (Beijing, China). All antibodies used in this study were purchased from Affinity Biosciences (Cincinnati, Ohio, USA).

2.2. Preparation of oxidized pullulan

Periodate oxidation was used to selectively oxidize and break the dihydroxy or trihydroxy positions in the pullulan molecules, generating corresponding polysaccharide aldehyde groups [35–37]. In short, Dissolve 1 g of pullulan in 50 mL of deionized water, then add 1.98 g of sodium periodate, and induce an oxidation reaction at room temperature for 4 h to obtain oxidized pullulan solution. Afterward, the oxidation reaction was stopped by dropping 1 mL of ethylene glycol, and the reaction mixture was dialyzed for another 3 d and freeze-dried to obtain oxidized pullulan (OP).

2.3. Preparation of hydrogels

Firstly, gelatin, OP, and blackcurrant extract were dissolved in PBS solution to obtain 120 mg/mL gelatin solution, 40 mg/mL and 20 mg/mL OP solution, as well as 40 mg/mL, 20 mg/mL, and 4 mg/mL blackcurrant extract solution. First, a 1:1 mixture of 120 mg/mL gelatin solution and 20 mg/mL OP solution yielded the gelatin-OP hydrogel, denoted as G-O. Next, combining 120 mg/mL gelatin solution, 40 mg/mL OP solution, and 40 mg/mL blackcurrant extract solution in a 2:1:1 ratio resulted in the gelatin-OP-blackcurrant extract hydrogel, abbreviated as G-*O*-B. The final concentrations of blackcurrant extract in G-*O*-B hydrogels were 10 mg/mL, 5 mg/mL, and 1 mg/mL, respectively. To differentiate and describe them conveniently, these hydrogels were named G-*O*-$B_{1.0}$, G-*O*-$B_{0.5}$, and G-*O*-$B_{0.1}$.

2.4. SEM observation

300 μL G-O and G-*O*-B hydrogels were prepared in 1.5 mL EP tubes, freeze-dried with a freeze dryer, brittle fracture with liquid nitrogen, sprayed with gold, observed and photographed with a scanning electron microscope (SEM, FEIQuanta200, Netherlands).

2.5. In vitro stability test

In vitro, stability experiments of hydrogels were based on the published protocol [38]. Briefly, 100 μL of the hydrogels were prepared. Each hydrogel was placed in a pre-weighed 2 mL centrifuge tube, with the weight of an empty tube recorded as W_{blank} and the total weight of the hydrogel and tube as $W_{day\ 0}$. Subsequently, 2 mL of PBS solution was added, and the tube was placed in a 37 °C water bath. On days 2, 4, 6, 8, 10, and 12, the PBS solution was decanted from the tube, and any remaining PBS around the hydrogel was blotted with absorbent paper. The total weight of the hydrogel and tube was recorded as $W_{day\ n}$. The residual weight of the hydrogel was calculated using the formula to evaluate and analyze the *in vitro* stability. The calculation formula is as follows: the weight of the remaining hydrogel (%)=($W_{day\ n}$-W_{blank})/($W_{day\ 0}$-W_{blank}) × 100 %.

The hydrogels were immersed in PBS for 1, 2, 3, 6, and 12 h, and the swelling rate curve was measured. The swelling rate was calculated by dividing the weight after immersion in water by the initial weight and then multiplying the result by 100 %.

2.6. Injectability and shape-adaptability

The injectability of hydrogel was assessed as follows: the G-*O*-$B_{0.5}$ hydrogel was loaded into a syringe, squeezed to form the letter "ZZU", and then injected into deionized water to observe its behavior.

The shape-adaptability of hydrogel was carried out based on the previous report [39]. Preparation of 500 μL G-*O*-$B_{0.5}$ hydrogel and injected into the mold. After the hydrogel is stable, take out the shaped hydrogel for visual observation and photographic record.

2.7. Photothermal testing

The near-infrared (NIR) light with a wavelength of 808 nm and a power of 2.5 W/cm^2 was used to irradiate each group of hydrogels for 10 min. The infrared thermal imager (T120, Guide) was used to test and record the temperature every 30 s to explore and analyze the photothermal conversion capacity of hydrogel in each group.

2.8. Rheological test

The rheological property of G-*O*-B hydrogel were assessed by determining the elastic modulus of 2 mL cylindrical hydrogel using a rheometer (Leica DHR2, Germany). Parameters were standardized as follows: oscillation sweep frequency at 1 Hz, angular frequency ranging from 0.1 to 100 rad/s, temperature set at 37 °C, and strain maintained at 1 %. Subsequently, the energy storage modulus (G') and loss modulus (G″) of each hydrogel sample were measured and recorded.

2.9. Inherent antibacterial test

The inherent antibacterial property of hydrogel was evaluated based on our previous literature [40]. In summary, 200 μL of G-O and G-*O*-B hydrogels were prepared and dispensed into a 24-well plate. Then, 10 μL of bacterial suspension (*Escherichia coli*, *Staphylococcus aureus*, and *Pseudomonas aeruginosa* at a concentration of 10^7 CFU/mL) was added onto the hydrogel surface, while the control group received direct addition of 10 μL bacterial suspension per well. After 6 h of incubation, each well was resuspended with 1 mL of bacterial culture medium, and 100 μL from each well was transferred to fresh culture medium for further incubation for 18–24 h. The absorbance at 600 nm was measured using a microplate reader to assess the live bacterial count and determine the inherent antibacterial activity. Additionally, to further explore the antibacterial property of G-*O*-B hydrogel material, the antibacterial effectiveness of gelatin, OP, and three different concentrations of blackcurrant extract against *Escherichia coli*, *Staphylococcus aureus*, and *Pseudomonas aeruginosa* was also evaluated.

2.10. NIR-assisted antibacterial test

The NIR-assisted antibacterial activity of hydrogels were tested according to the previous literature method [41]. Under sterile condition, 200 μL of G-*O*-$G_{0.5}$ hydrogels were prepared and transferred in a 24-well plate. Then add 10 μL of bacterial suspension with a concentration of 10^7 CFU/mL onto the surface of each hydrogel, and add another 10 μL equal bacterial suspension into the blank well as the control group. The hydrogel was irradiated with NIR (808 nm 2.5 W/cm^2) for 0, 1, 3, 5, and 10 min. Subsequently, the viable bacteria were resuspended in 1 mL of liquid medium, with 100 μL of suspensions aspirated into 1 mL of liquid medium from each group. After 18–24 h of incubation, the absorbance of the culture medium was measured at 600 nm using a microplate reader to assess bacterial viability. Subsequently, 100 μL was plated onto solid AGAR medium. The AGAR plates were then incubated at 37 °C for 18–24 h, and bacterial growth on the solid medium was observed and recorded.

2.11. Antioxidant assays

The Safranin O antioxidant assay was used to determine the reactive oxygen species (ROS) scavenging ability of hydrogel according to our previous method [42]. ABTS radical scavenging assay was used to study the hydroxyl radical scavenging effect of G-*O*-B hydrogel according to our previous method [39].

The antioxidant capacity of the hydrogel was further evaluated using a cellular-level antioxidant assay. Mouse fibroblasts (L929) were seeded into a 96-well plate and cultured for 24 h before replacing the medium with fresh culture medium containing 0.5 mM H_2O_2 (the control group received fresh medium without H_2O_2) to induce oxidative stress. Simultaneously, 10 μL of hydrogel from each group was prepared. Each sterile hydrogel was added to the correspondent well containing the cultured cells, and after 2 h, the DCFH-DA dye solution was added and incubated for 20 min. The fluorescence intensity of each group was then recorded under a fluorescence-inverted microscope. Subsequently, the average fluorescence intensity of each group was calculated using Image J software.

2.12. Biocompatibility test

Blood compatibility experiment was conducted to assess the hemocompatibility of hydrogel. Mouse heart blood was collected into anticoagulant tubes. Subsequently, 50 μL of hydrogel was prepared for each group and placed into 1.5 mL centrifuge tubes, followed by the addition of 1 mL of normal saline to each tube. Simultaneously, positive control groups (1 mL of deionized water added to new centrifuge tubes) and negative control groups (1 mL of normal saline added to new centrifuge tubes) were set up. Afterward, all tubes were incubated in a 37 °C water bath for 30 min, and then 50 μL of blood was added to each centrifuge tube. Following a 1-h incubation at 37 °C, the hydrogel was removed, and the tubes were centrifuged at 1000 rpm for 5 min for photography and recording. Then suck the supernatant into a 96-well plate and measure the absorbance value at 545 nm. Finally, take photos under a microscope to record the status of each group of red blood cells. The formula involved is: Hemolysis ratio (%) = [($A_{hydrogel}$–$A_{negative}$)/($A_{positive}$–$A_{negative}$)] × 100 %.

The cytocompatibility of G-*O*-B hydrogel was determined according to the method previously reported [40]. First, inoculate L929 cells (at a density of 3.5 × 10^3 cells/well) into a 96-well plate and culture for 24 h. Meanwhile, prepare 100 μL of sterile hydrogel for each group and immerse 2 mL of cell culture medium in the hydrogel for 24 h to obtain the extract. Replace the culture medium of 96-well plate with the extract, and then incubate for 24 and 48 h, respectively. Replace the extract with fresh culture medium containing 10 % CCK8 (with a separate 10 % CCK8 solution as a blank control group). After an additional 2 h of cultivation, the absorbance value of each group at 450 nm

was measured by microplate reader, and then the cell viability was calculated according to the following formula: Cell viability (%) = $[(A_{hydrogel}–A_{blank})/(A_{control}–A_{blank})] \times 100$ %. Additionally, treat L929 cells with a culture medium containing 1 % Calcein AM/PI for 15 min. Observe and photograph the status and viability of cell in each group using a fluorescence-inverted microscope.

To investigate the histocompatibility of hydrogel, a subcutaneous embedding experiment was conducted as described previously [39]. The G-*O*-$B_{0.5}$ hydrogel was prepared under sterile condition. Subsequently, approximately 30 g Kunming mice were anesthetized, and 100 μL of the hydrogel was injected subcutaneously into the back of the mouse using a 1 mL syringe. After seven days, the mice were anesthetized again, and their heart blood was collected. Tissues were preserved by sequential injection of physiological saline and 4 % paraformaldehyde. The heart, liver, spleen, lungs, and kidneys were harvested, sectioned, and stained with hematoxylin and eosin (H&E) to observe and analyze potential infiltration of inflammatory cells and tissue lesions. Additionally, the collected heart blood was used to detect enzyme activity using kits for alanine aminotransferase (GPT), aspartate aminotransferase (GOT), and alkaline phosphatase (AKP) to evaluate overall mouse health.

2.13. Hemostatic performance test

The hemostatic performance of hydrogel was assessed using a mouse tail hemorrhage model and a liver hemorrhage model. In the mouse tail hemorrhage model, mice were anesthetized and immobilized, and a weighed filter paper was positioned beneath the tail. Using ophthalmic scissors, the tail was cut halfway. The control group received no treatment, while the hydrogel group was injected with 100 μL of G-*O*-$B_{0.5}$ hydrogel at the tail breakage site immediately. Photos were taken and bleeding cessation was noted. The filter paper was then weighed. For the hepatic hemorrhage model, anesthetized and immobilized mice had their livers exposed with surgical scissors. Tissue fluid was carefully removed using filter paper, and a weighed filter paper was placed under the liver. An 8 mm wound was created. Again, the control group received no treatment, while the hydrogel group was injected with 100 μL of hydrogel simultaneously with the wound creation. Photos were taken once blood coagulated, and the filter paper weight was measured.

The *in vitro* coagulation property of hydrogel was investigated according to the method previously reported [39]. Simply, add 10 μL 0.2 M $CaCl_2$ solution to 1 mL of mouse blood to obtain calcified blood. Then 250 μL G-*O*-$B_{0.5}$ hydrogel was placed in a 24-well plate, and then 25 μL calcified blood drops were added to the surface of the hydrogel. In the control group, 25 μL calcified blood was directly added to the plate. Then immediately incubate in a 37 °C water bath for 30 s, 60 s, 120 s, 180 s, 300 s, and 600 s, and then add 2.5 mL of deionized water to suspend the unattached blood. Then measure the absorbance value of the supernatant (the optical density of free hemoglobin in the system) at 540 nm. The hydrogel group used A_h, the blank group (deionized water) used A_b, and the control group used A_v and calculated the blood coagulation index (BCI) using the following formula: BCI (%) = $[(A_h–A_b)/(A_v–A_b)] \times 100$ %.

2.14. Establishment of a deep secondary burn and Staphylococcus aureus infection model in Kunming mice

For the construction of deep secondary burn model, Kunming mice aged around 6 weeks and weighing approximately 30 g were selected. The handling and treatment of the animals followed the protocol approved by the Ethics Committee of Zhengzhou University. One week before the experiment, the mice were randomly divided into four groups and allowed free access to food. To create the burn models, the previously reported method was followed [43]. The mice were initially anesthetized and their dorsal hair was shaved. Afterward, a benchtop hypertemperature-controlled burn instrument (YLS-5Q) set at 90 °C, a pressure of 250 g was applied for 5 s to create a circular burn wound with a diameter of 8 mm over the shaved area. Immediately after the burn, 100 μL of physiological saline was injected into the peritoneal

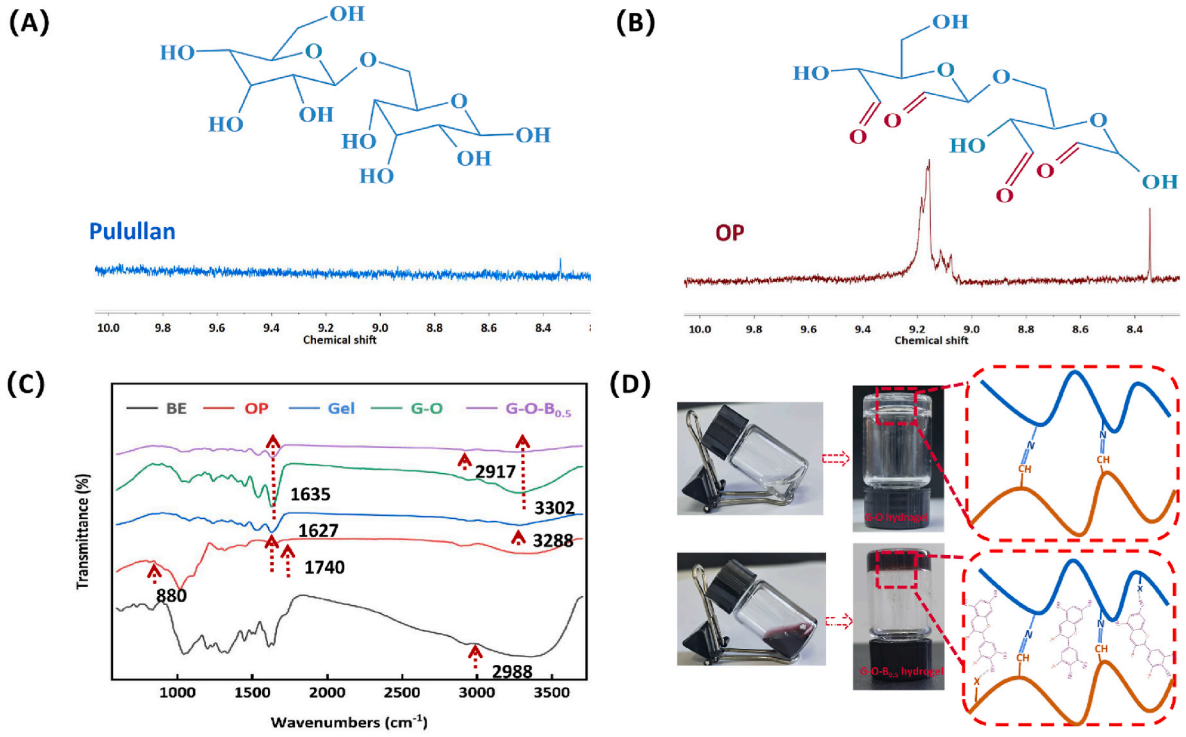

Fig. 1. Synthesis and spectral analysis of OP and G-*O*-B hydrogel. ^{1}H NMR spectra and structural formula of (A) pullulan and (B) oxidized pullulan (OP); (C) FTIR spectra of blackcurrant extract (B), OP, gelatin, G-O hydrogel, G-*O*-$B_{0.5}$ hydrogel; (D) Photographs of G-O hydrogel and G-*O*-$B_{0.5}$ hydrogel formation process and diagram of hydrogel cross-linking mechanism.

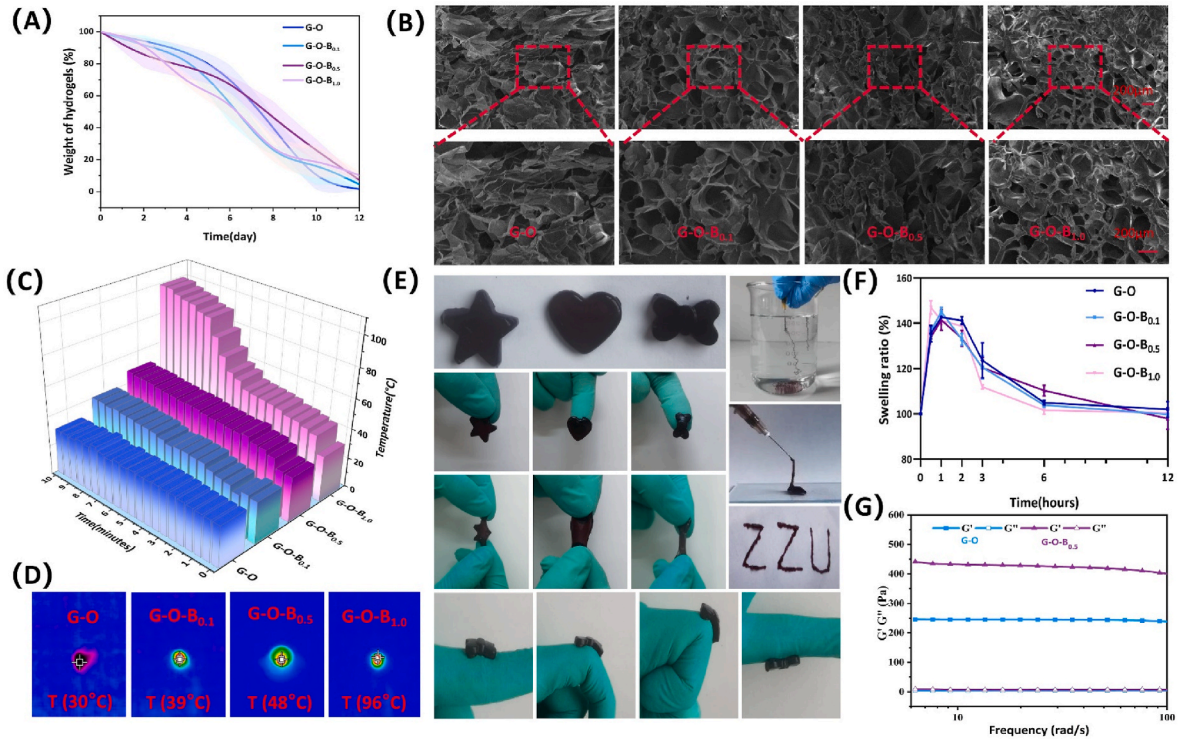

Fig. 2. Characterization of hydrogel properties. (A) *In vitro* stability of G-O hydrogel, G-*O*-$B_{0.1}$ hydrogel, G-*O*-$B_{0.5}$ hydrogel and G-*O*-$B_{1.0}$ hydrogel; (B) SEM images of each hydrogel; (C) Temperature change maps of hydrogels in each group after NIR irradiation for 10 min (808 nm, 2.5 W/cm^2); (D) Real-time thermal maps of hydrogels after 10 min of irradiation; (E) Photographs of shape-adaptability and injectability of G-*O*-$B_{0.5}$ hydrogel; (F) Swelling behavior of hydrogel in each group; (G) Rheological data of G-O and G-*O*-$B_{0.5}$ hydrogels. Mean ± SD, n = 3.

cavity to aid recovery and prevent dehydration. After 24 h, debridement was performed on the burn wound using surgical scissors to remove necrotic tissue. Subsequently, 50 μL of *Staphylococcus aureus* (10^7 CFU/mL) was applied to induce infection for 2 h. This protocol successfully established a deep secondary and infected burn model in Kunming mice, aiming to assess the impact of hydrogel treatment on wound healing in this specific burn model.

2.15. Hydrogel treatment

After bacterial infection, the four groups of mice were treated as follows: the control group received no treatment, the G-O hydrogel group covered with 100 μL of G-O hydrogel, the NIR-group covered with 100 μL of G-*O*-$B_{0.5}$ hydrogel without treatment, and the NIR + group covered with 100 μL of G-*O*-$B_{0.5}$ hydrogel and NIR treatment. Following the injection of 100 μL of G-*O*-$B_{0.5}$ hydrogel, mice in the NIR + group underwent NIR irradiation at a power density of 2.5 W/cm^2 for 10 min. Concurrently, near-infrared thermal imaging was employed to monitor and maintain the temperature within the range of 45–50 °C. The other hydrogel group only received a 100 μL hydrogel application. This experimental design facilitated the comparison and assessment of the efficacy of the four different treatment regimens in wound healing.

2.16. Evaluation of wound healing

The wound healing progress in each experimental group was systematically monitored and documented through observation and photography on days 1, 3, 7, and 14 post-treatment. Additionally, on day 7, wound tissues were collected for immunofluorescence staining to evaluate the expression of CD31, α-SMA, CD86, and CD206 for inflammatory response and angiogenesis. Skin wound tissue samples from each group were then obtained on day 14 for histological analysis using H&E and Masson stainings. These histological methods facilitated the examination and assessment of tissue morphology, cellular composition, and collagen deposition within the wound site.

2.17. Evaluation of infection

On day 3, wound tissue samples were collected from each group and homogenized. Subsequently, 2 mL of liquid medium was added to the homogenates, and the resulting solutions were cultured for 16–24 h at 37 °C. After that, the culture medium was subjected to a 10,000-fold dilution. A 100 μL aliquot of the diluted medium was then plated onto agar plates and incubated for an additional 16–24 h. The resulting colonies were photographed, and the antibacterial efficacy of each experimental group was evaluated.

2.18. Statistical analysis

All experiments were repeated at least three times, and the results were determined as mean ± standard deviation (SD). GraphPadPrism8 was used for statistical analysis, and the Tukey method was used to test the results of one-way or two-way ANOVA, with $p < 0.05$ representing the level of significant difference.

3. Results and discussion

3.1. Fabrication and gelation mechanism of G-O-B hydrogels

To obtain oxidized pullulan (OP), some hydroxyl groups on pullulan were oxidized to aldehyde groups by sodium periodate. From the ^{1}H NMR spectrum in Fig. 1A and B, an identified new peak of 9.27 ppm was witnessed corresponding to the aldehyde group in OP [44,45]. Based on Fig. S1, the oxidation rate of pullulan in OP was calculated to be between 10 % and 15 %. To gain insight into the gel-formation mechanism, FTIR spectral analysis of gelatin, blackcurrant extract (B), freeze-dried OP,

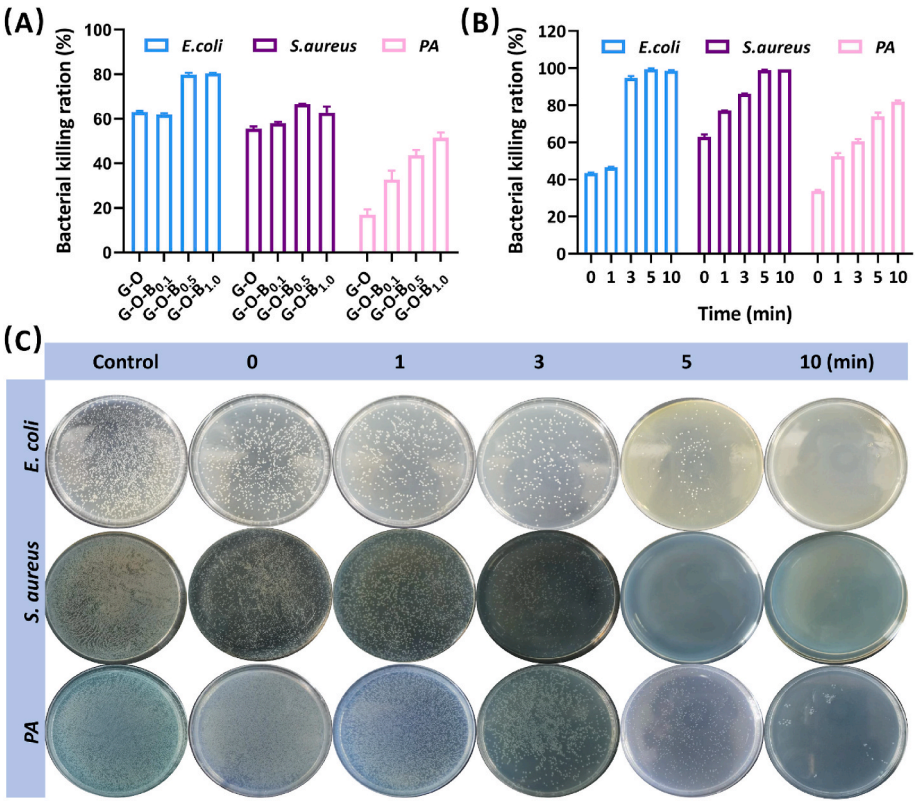

Fig. 3. Antibacterial activity of G-*O*-B hydrogel. (A) The inherent antibacterial rate of G-O hydrogel, G-*O*-$B_{0.1}$ hydrogel, G-*O*-$B_{0.5}$ hydrogel, and G-*O*-$B_{1.0}$ hydrogel against *Escherichia coli*, *Staphylococcus aureus*, and *Pseudomonas aeruginosa*; (B) The photothermal killing rate of G-*O*-$B_{0.5}$ hydrogel against *Escherichia coli*, *Staphylococcus aureus*, and *Pseudomonas aeruginosa* after 0, 1, 3, 5 and 10 min of NIR irradiation; (C) Photographs of *Escherichia coli*, *Staphylococcus aureus*, and *Pseudomonas aeruginosa* colonies on AGAR plates after 0, 1, 3, 5 and 10 min of NIR irradiation. Mean ± SD, n = 3.

G-O hydrogel, and G-*O*-$B_{0.5}$ hydrogel were analyzed. Fig. 1C illustrates that the majority of aldehyde groups undergo interaction with amino groups to form imine bonds in the G-O hydrogel and G-*O*-$B_{0.5}$ hydrogel structures, thus causing the characteristic peak of aldehyde group at 1740 cm^{-1} to become less prominent [46]. In contrast, the characteristic peak of aldehyde group in the OP group remains unaffected. The peak at 1635 cm^{-1} indicates the presence of imine bonds in both hydrogel groups [47,48]. Additionally, G-O and G-*O*-$B_{0.5}$ have a peak at 3302 cm^{-1} corresponding to N–H tensile vibration, while gelatin has a peak at 3288 cm^{-1}. The N–H stretching peak width of G-O and G-*O*-$B_{0.5}$ is smaller than that of gelatin, suggesting the formation of imine groups between amino and aldehyde groups [49]. Furthermore, the absorption band at 2988 cm^{-1} corresponds to the –OH tensile vibration of B, which shifts to 2917 cm^{-1} after gelation in the G-*O*-$B_{0.5}$ hydrogel group, indicating the formation of hydrogen bonding during the gelation process [50,51]. In summary, G-O and G-*O*-B hydrogels are crosslinked via the Schiff base reaction. Additionally, for G-*O*-B hydrogel, the phenolic hydroxyl groups present in B can engage in intermolecular hydrogen bonding with gelatin and OP to form another hydrogel interpenetrating network (refer to Fig. 1D).

3.2. Stability, SEM, shape-adaptability, injectability, and photothermal properties of G-O-B hydrogels

Stability is one of the important indicators in evaluating hydrogel wound dressings [52]. Appropriate stability can not only ensure that the hydrogel dressing continues to play a protective role until the skin is completely healed but also avoid secondary injury to the wound caused by the hydrogel removal process. According to the data in Fig. 2A, the hydrogel in each group gradually degraded over time, and their stability remained for more than 12 days, close to the skin wound healing period.

From the scanning electron microscope (SEM) images in Fig. 2B, it can be seen that both G-O and G-*O*-B hydrogels present a clear three-dimensional network structure. Besides, with the growth of B content, the crosslinking density of the hydrogel network increased, and the pore size gradually decreased. This connected three-dimensional network structure makes the hydrogel highly absorbent (Fig. 2F), which can effectively absorb the exudate in the burn wound, and form a scaffold structure at the wound, providing a positive environment for cell growth and wound healing [53–55].

This study employed an 808 nm near-infrared (NIR) laser (2.5 W/cm^2) and thermal imaging instrument to examine the photothermal stability of G-*O*-B hydrogel. Fig. 2C illustrates that with increasing irradiation time, the temperature of the G-O hydrogel group without extract remains relatively constant, while that of the extract-loaded hydrogel group gradually increases, indicating a positive correlation between temperature and extract content. Fig. 2D depicts the thermal image of hydrogels in each group after 10 min of NIR irradiation. Following this period, the temperature of the G-O, G-*O*-$B_{0.1}$, G-*O*-$B_{0.5}$, and G-*O*-$B_{1.0}$ hydrogels reached approximately 30 °C, 39 °C, 48 °C, and 96 °C, respectively. Moreover, throughout the experiment, it was observed that except for the G-*O*-$B_{1.0}$ hydrogel group, which experienced significant water loss due to evaporation at high temperatures, the other hydrogel groups exhibited minimal changes in water loss and volume after 6 min of NIR irradiation. These results suggest that such hydrogel possesses favorable and adjustable characteristics. Notably, the G-*O*-B hydrogel demonstrated distinct temperature controllability for anthocyanins (a constituent of blackcurrant extract) release. Based on the color of the released hydrogel and the light absorption value at 580 nm (Fig. S2), it is evident that anthocyanin release at 45 °C is significantly faster than that at 37 °C and 25 °C. This attribute also endows the G-*O*-B hydrogel with smart wound-dressing capabilities.

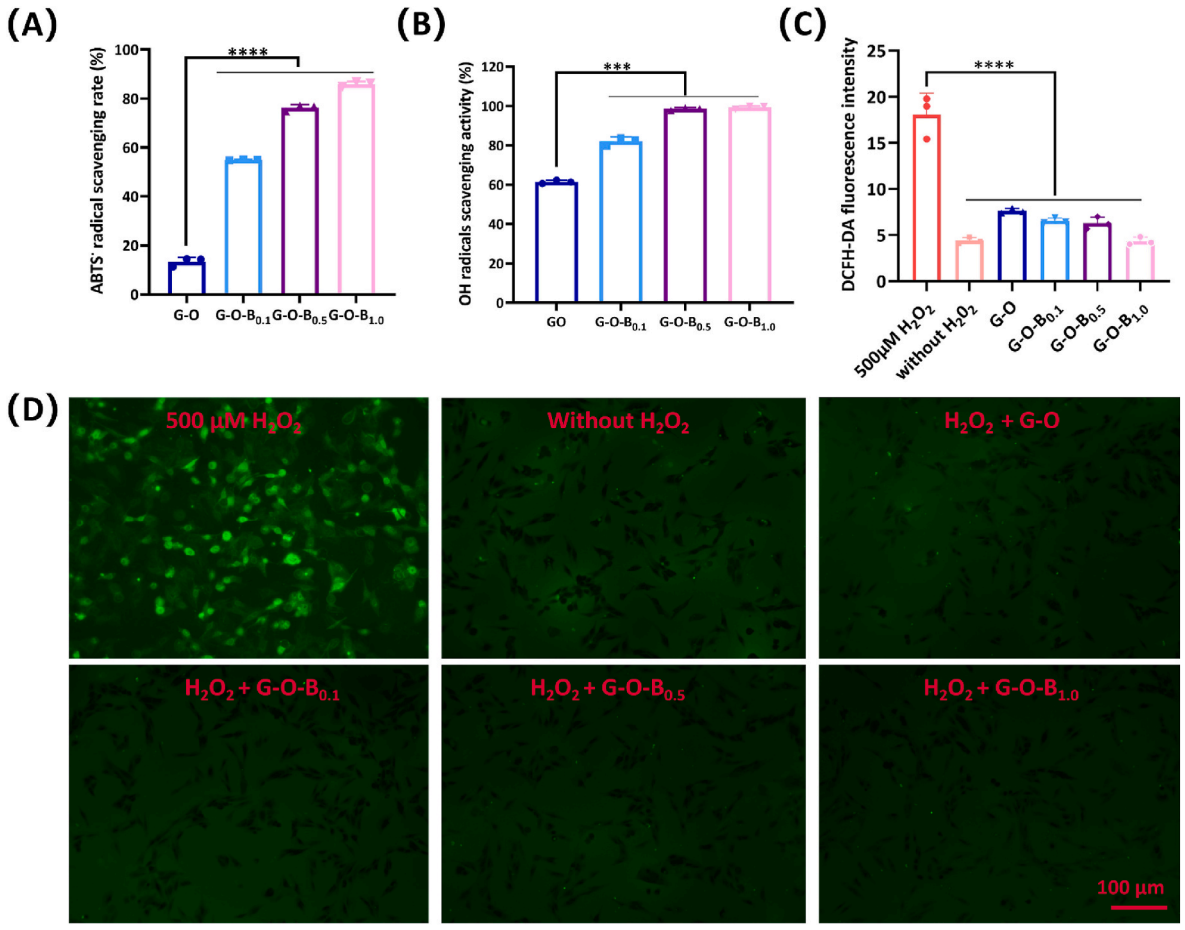

Fig. 4. The antioxidant capacity of G-O and G-*O*-B hydrogels. (A) ABTS radical clearance rate; (B) Hydroxyl radical clearance by safranine O assay; (C) Statistical analysis of DCF fluorescence intensity in each group, (D) Fluorescence staining images of L929 cells treated with or without 500 μM H_2O_2 for 2 h and treated with or without 10 μL hydrogel in each group, ***$p < 0.001$, ****$p < 0.0001$, mean ± SD, n = 3.

The extraordinary flexibility and adaptability of G-*O*-$B_{0.5}$ hydrogel shown in Fig. 2E allows it to be effectively adapted to various wound shapes and sizes, thereby mitigating further damage. Additionally, it possesses substantial adhesive strength, facilitating close adherence to the burn wound surface, ensuring stability, and preventing displacement or detachment. Furthermore, the injectability of this hydrogel suggests its suitability for various types and shapes of wounds. The injection volume and injection method can be adjusted according to the size and depth of the wound, which enhances its versatility and applicability in wound treatment [56,57]. Injecting the hydrogel into the wound facilitates rapid absorption of wound exudate, enhancing adsorption and penetration at the wound site. This property creates a moist environment conducive to wound healing, reducing pain and offering advantages over conventional wound dressings. The stability, shape adaptability, and injectability of the G-*O*-B hydrogel dressing contribute significantly to its prolonged effectiveness, particularly for burn wounds. Utilizing this dressing is anticipated to decrease dressing change frequency, alleviate patient discomfort, and potentially improve therapeutic outcomes.

The mechanical property of G-*O*-B hydrogel was also investigated through rheological analysis (Fig. 2G). At angular frequencies ranging from 10 to 100 rad/s, G′ consistently surpassed G", indicating a gel-like behavior akin to solids. Furthermore, the incorporation of B resulted in a rise of G' from 245 Pa to 441 Pa at 100 rad/s. This observation is likely attributed to the formation of intermolecular hydrogen bonds between B and gelatin/OP. The increased number of hydrogen bonds within the G-*O*-B hydrogel system leads to a noticeable enhancement in its mechanical strength.

3.3. Inherent antibacterial and photothermal antibacterial activity of G-O-B hydrogels

Burn wounds are highly susceptible to infection due to the destruction of skin barriers and blood vessels, as well as other factors such as bacterial presence and nutrients in the burn environment [58]. Wound infection is a common complication in burn wounds, which can worsen inflammation [59]. Additionally, the presence of bacteria and pathogens can lead to tissue necrosis at the wound edges, further damaging local tissue and hindering wound recovery [60]. The antibacterial activity of G-*O*-B hydrogel against three common bacteria (*Escherichia coli*, *Staphylococcus aureus*, and *Pseudomonas aeruginosa*) prevalent in burn wounds was studied. Fig. 3A displays the antibacterial rates of hydrogels in each group following a 6-h contact period with the bacterial solution. Overall, the inclusion of blackcurrant extract containing polyphenols enhanced the hydrogel's antibacterial effect. Specifically, the antibacterial rates against *Escherichia coli* ranged from 62.4 % to 80.49 %, against *Staphylococcus aureus* from 54.4 % to 65.4 %, and against *Pseudomonas aeruginosa* from 18.4 % to 52.6 %. These results demonstrate the good antibacterial property of G-*O*-B hydrogel, likely attributed to the presence of blackcurrant extract and oxidized pullulan [61]. It has been reported that blackcurrant extract contains anthocyanins and flavonoids, which are known for their antioxidant and antibacterial properties. These bioactive compounds have been shown to possess inhibitory effects on various types of bacteria [62–64]. The antibacterial results of each component of the hydrogel are shown in Fig. S3, which also confirms the antibacterial mechanism of G-*O*-B hydrogel.

Recently, photothermal antibacterial agents have gained widespread

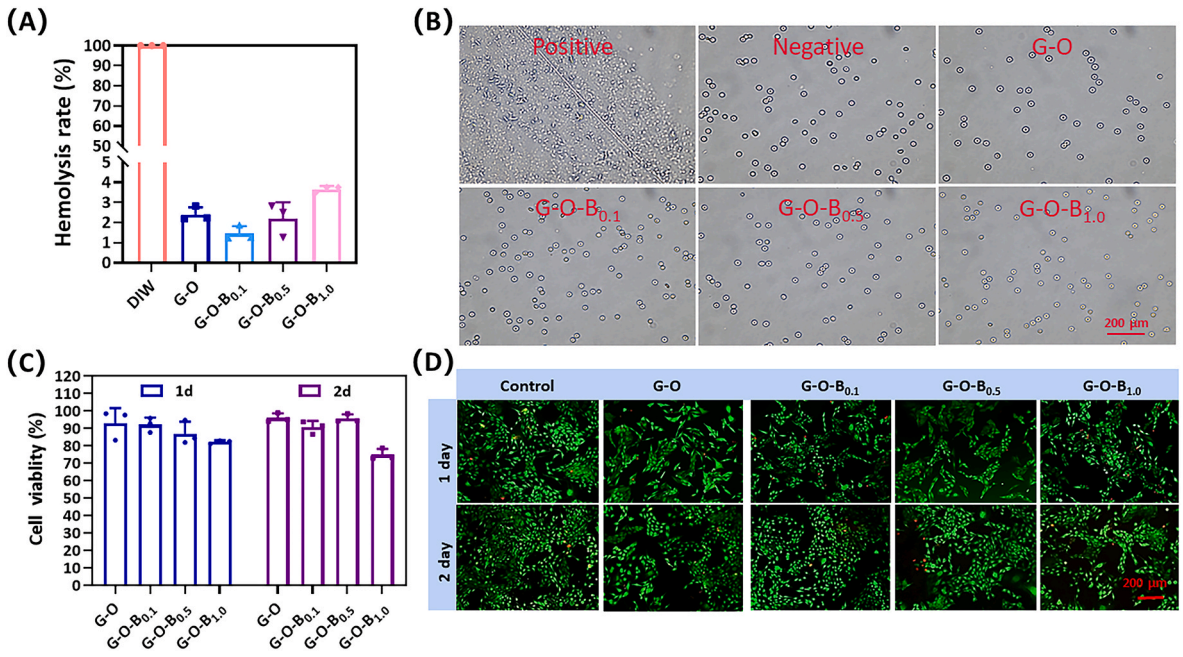

Fig. 5. Hemolytic property and *in vitro* cytocompatibility of G-O hydrogel, G-*O*-$B_{0.1}$ hydrogel, G-*O*-$B_{0.5}$ hydrogel, and G-*O*-$B_{1.0}$ hydrogel. (A) Hydrogel hemolysis rate in each group and (B) photos of red blood cells after hydrogel treatment in each group; (C) CCK-8 assay of activity of L929 cells incubated with hydrogel extract for 1 and 2 days; (D) Live/dead fluorescent staining images of L929 cells on day 1 and day 2. Mean ± SD, n = 3. (For interpretation of the references to color in this figure legend, the reader is referred to the Web version of this article.)

use in fields such as food, medicine, and environmental health due to their efficient antibacterial effect, lack of chemical residue, and absence of drug resistance [65,66]. Compared to traditional high-temperature sterilization methods, NIR antibacterial technology can be conducted at lower temperatures, thus avoiding the destruction of other active ingredients present in wound dressings. In this study, based on the stability, injectability, and photothermal properties of G-*O*-B hydrogels, G-*O*-$B_{0.5}$ hydrogel was selected for further evaluation of the photothermal antibacterial effect. As shown in Fig. 3B, with the extension of NIR irradiation time, the antibacterial rate of G-*O*-$B_{0.5}$ hydrogel gradually increased. After 10 min of irradiation, the inhibition rate of the hydrogel against *Escherichia coli* and *Staphylococcus aureus* reached about 98 % and 99 %, and the inhibition rate against *Pseudomonas aeruginosa* was also over 82 %. Furthermore, the efficacy of G-*O*-$B_{0.5}$ hydrogel was corroborated in Fig. 3C via AGAR plate culture for the aforementioned bacteria post-irradiation at different intervals. With NIR irradiation, the time taken by G-*O*-$B_{0.5}$ hydrogel to eradicate bacteria was notably shortened from 6 h to 10 min, potentially mitigating the risk of infection and inflammation. Consequently, this photothermal G-*O*-B hydrogel exhibits promising prospects for advancing wound healing via swift antibacterial action.

3.4. Antioxidant activity of G-O-B hydrogels

Blackcurrant extract has been reported to contain a variety of nutrients and antioxidants, including anthocyanins, vitamin C, and phenolic compounds [67]. Due to its potent antioxidant and immune regulatory properties, this natural plant extract finds widespread applications in health products, cosmetics, and medicines [32]. Our findings indicate that the ability of hydrogel to scavenge free radicals is enhanced as the concentration of blackcurrant extract increases (Fig. 4A and B). Specifically, the ABTS free radical scavenging rates by the G-O, G-*O*-$B_{0.1}$, G-*O*-$B_{0.5}$, and G-*O*-$B_{1.0}$ hydrogels were found to be 14.4 %, 55.2 %, 76.8 %, and 86.2 %, respectively. The clearance rates for hydroxyl free radicals of these hydrogels were 61.3 %, 82.9 %, 98.1 %, and 99.7 %, respectively. To assess the antioxidant capacity of hydrogel at cellular level, we employed 2′,7′-dichlorodihydrofluorescein diacetate (DCFH-DA) as a probe to measure intracellular ROS level. When L929 cells were co-cultured with 500 μM H_2O_2 for 2 h, intense green fluorescence indicative of ROS production was observed (Fig. 4C and D). Conversely, the cells treated with hydrogel resulted in a significant decrease in fluorescence intensity in each group ($p < 0.0001$). The effectiveness of the G-*O*-B hydrogel in demonstrating the removal of reactive oxygen species (ROS) and providing cellular protection from oxidative damage suggests that the G-*O*-B hydrogel has the potential as a treatment option for mitigating oxidative stress, inflammation, and the generation of free radicals.

3.5. Biocompatibility of G-O-B hydrogels

Hydrogels are biomaterials that offer significant advantages in terms of biocompatibility, which has led to their widespread usage in the fields of medicine and bioengineering [68,69]. In this study, the biocompatibility of G-*O*-B hydrogel was systematically examined by evaluating its blood compatibility, cell compatibility, and histocompatibility.

Blood compatibility is an important indicator when considering the potential application of biomaterials in a blood environment [70]. According to the International Standards for Biomedical Materials (ISO70:10993), suitable biomedical materials should maintain stable chemical and physical properties when in contact with blood, while avoiding abnormal biological reactions [71]. To ensure safety and effectiveness in the blood environment, the percentage of hemolysis should not exceed 5 % [39]. Fig. 5A demonstrates that the supernatant of the hydrogel in each group was clarified with no evident signs of hemolysis. The hemolysis rates of G-O, G-*O*-$B_{0.1}$, G-*O*-$B_{0.5}$, and G-*O*-$B_{1.0}$ hydrogels were found to be 2.23 %, 1.27 %, 2.51 %, and 3.76 %, respectively. Additionally, Fig. 5B illustrates the microscopic observations of red blood cell morphology in each group. These findings collectively confirm that G-*O*-B hydrogel does not cause the rupture or deformation of red blood cells, indicating its good blood compatibility.

Hydrogel materials play an important role in maintaining the normal morphology and specific phenotype of cells, which is essential for their metabolic and functional expression, as well as proliferation and growth [70]. In this study, we evaluated the cytocompatibility of G-*O*-B

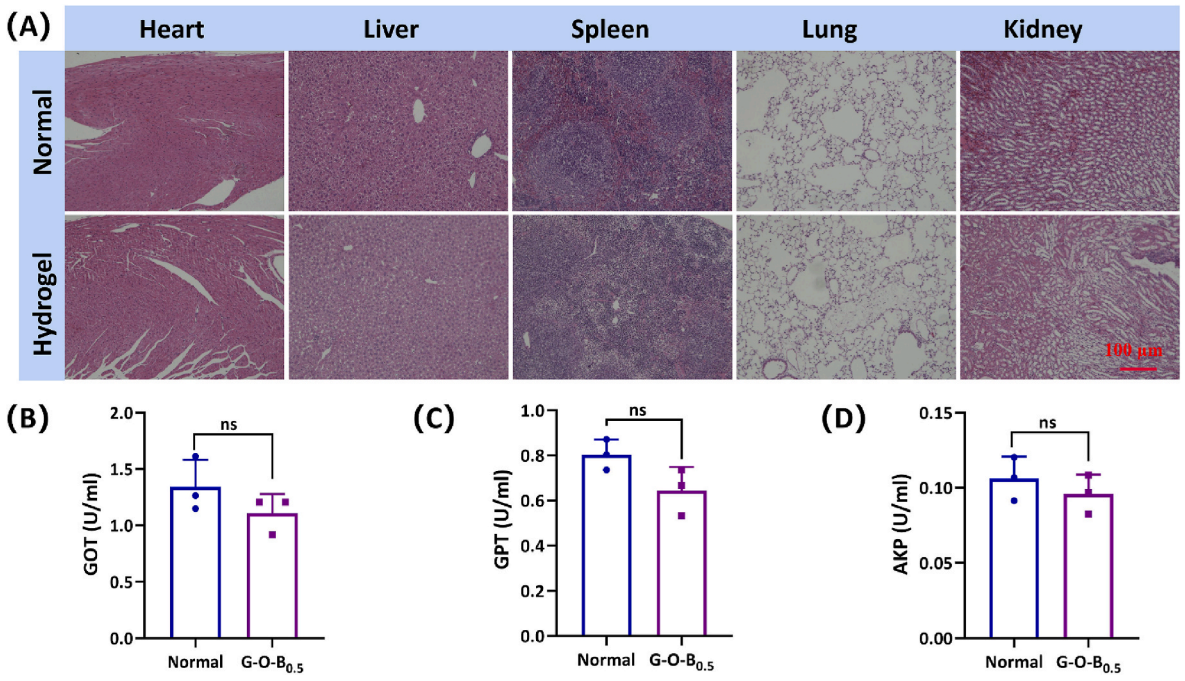

Fig. 6. Biocompatibility of G-*O*-$B_{0.5}$ hydrogel *in vivo*. (A) H&E staining images of main organs of normal mice and hydrogel-implanted mice on the 7th day; Blood biochemical analysis of serum GPT (B), GOT (C), and AKP (D) in each group on the 7th day. Mean ± SD, n = 3, $p > 0.05$.

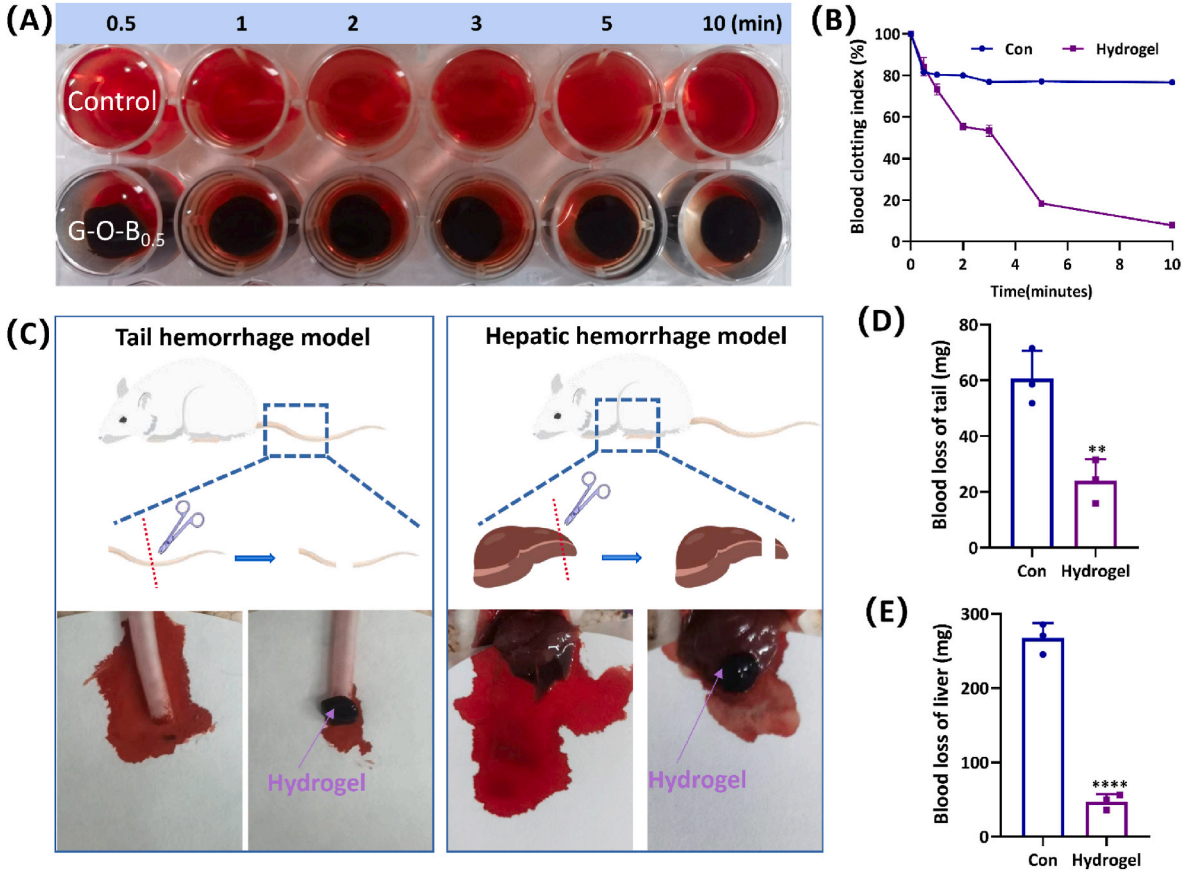

Fig. 7. Blood coagulation *in vitro* and hemostasis *in vivo* of G-*O*-$B_{0.5}$ hydrogel. (A) Photographs of the coagulation test of G-*O*-$B_{0.5}$ hydrogel; (B) BCI at specified time points of the control group and hydrogel group; (C) Schematic diagram of tail bleeding model and liver incision model, photographs of blood stains, untreated (control group), blood loss treated with hydrogel; (D) Tail blood loss statistics in each group; (E) Liver blood loss statistics in each group. **$p < 0.01$, ****$p < 0.0001$, mean ± SD, n = 3.

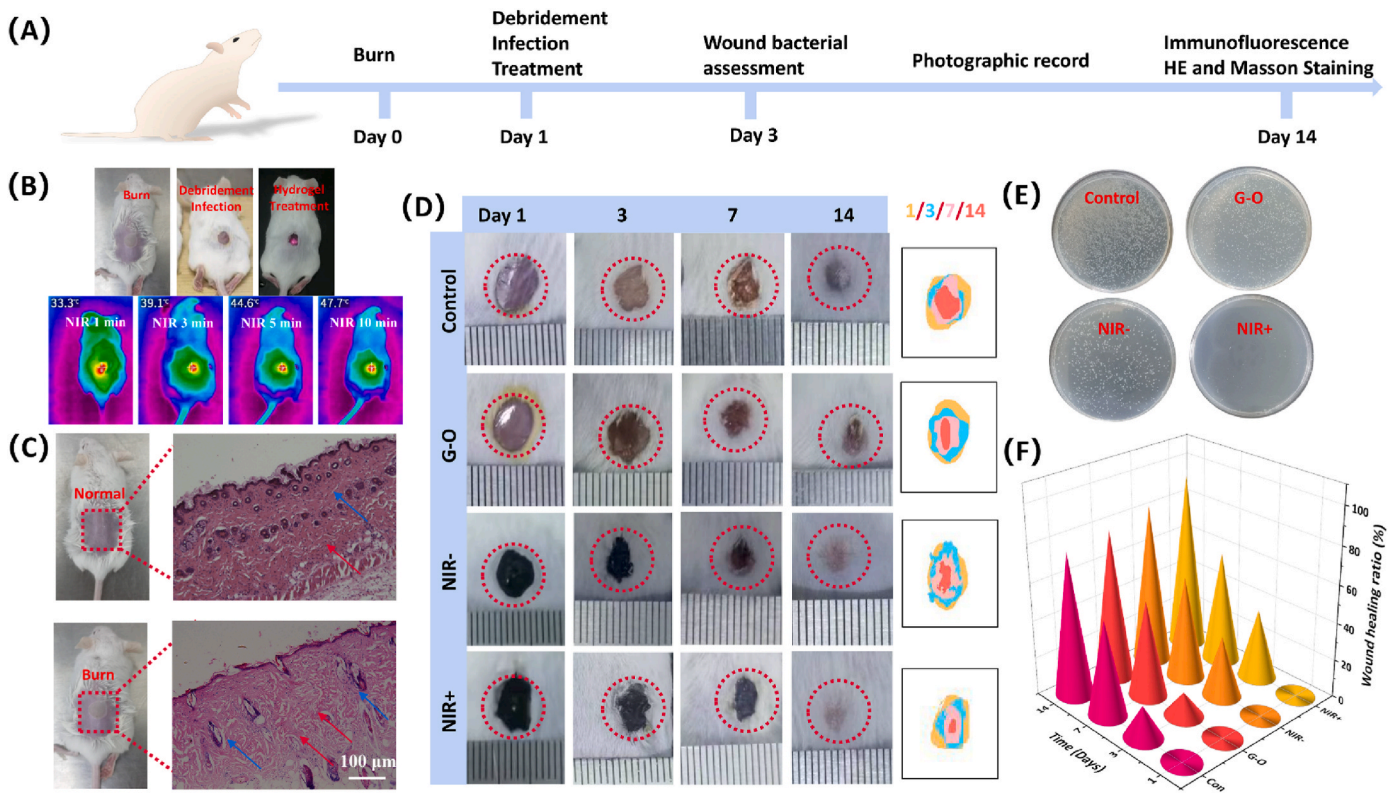

Fig. 8. Effect of G-*O*-$B_{0.5}$ hydrogel on healing of skin burn wound infected by *Staphylococcus aureus* in a mouse model. (A) and (B) Schematic diagram of burn infection wound modeling and treatment; (C) H&E staining on the skin of normal mice and mice with deep second-degree burn; (D) Photographs and wound shrinkage maps of the healed wounds on days 1, and 3, 7, 14 in each group; (E) Detection of *Staphylococcus aureus* colonies on coated AGAR plate for analysis of wound infection on day 3; (F) Wound healing rate in each group. Mean ± SD, n = 3.

hydrogel using commonly employed methods, including CCK8 assay and live/dead fluorescent staining. As depicted in Fig. 5C, the survival rates of L929 cells in the G-O, G-*O*-$B_{0.1}$, G-*O*-$B_{0.5}$, and G-*O*-$B_{1.0}$ hydrogel groups were found to be higher than 70 %, which meet the International Standards for Biological Materials [72]. Besides, the strong green fluorescence observed in Fig. 5D indicates that cells from all groups were specifically labeled as viable cells. Based on these results, we conclude that all tested hydrogels exhibit good biocompatibility with L929 cells.

The histocompatibility of a hydrogel refers to its ability to interact with and adapt to the surrounding tissues [73]. Good histocompatibility means that the hydrogel can be compatible with the surrounding tissues without causing excessive inflammation or immune response while promoting tissue regeneration and repair [74]. It is also an important indicator for evaluating hydrogels as biomedical materials. The hematoxylin and eosin (H&E) staining images in Fig. 6A show that compared with normal mice, no discernible pathological changes or inflammatory cells were observed in the tissues of hydrogel-injected mice (7 days after subcutaneous injection). The data in Fig. S4 present a favorable degradation behavior of G-*O*-$B_{0.5}$ hydrogel *in vivo*. These findings underscore the excellent histocompatibility and biodegradability of G-*O*-$B_{0.5}$ hydrogel.

Additionally, the levels of aspartate aminotransferase (GOT), alanine aminotransferase (GPT), and alkaline phosphatase (AKP) were not significantly different from those in the normal mouse group, as depicted in Fig. 6B–D. Overall, these outcomes illustrate the well biocompatibility of the hydrogel and its potential as a safe and efficient wound dressing.

3.6. Hemostatic activity of G-O-B hydrogels

Hemostasis is a crucial process in wound healing and treatment [75]. It is the earliest event that takes place in a wound, highlighting its importance. Hemostasis involves the promotion of blood clot formation at the wound site through the action of coagulation factors present in the blood [76]. This promotes the acceleration of wound healing. Wound dressings with hemostatic activity are recognized for their ability to support healing [77]. Hydrogel, as a hemostatic material, offers several advantages. It is typically soft, comfortable, and minimally irritating to the surrounding tissues. Additionally, hydrogel exhibits excellent water absorption capability, promptly absorbing blood and forming a gel-like state. The presence of coagulation factors in the hydrogel can also aid in preventing infection to a certain extent [78,79]. Consequently, hydrogel dressings help in controlling bleeding, promoting wound repair, and ultimately facilitating healing.

Studies have shown that plant extracts rich in polyphenols possess hemostatic effects [80]. Blackcurrant extract, being rich in polyphenols, has been investigated for its hemostatic effect. In this study, we explore the *in vitro* and *in vivo* hemostatic effect of blackcurrant extract-loaded hydrogels. The hemostatic ability of G-*O*-$B_{0.5}$ hydrogel was first assessed *in vitro*, as depicted in Fig. 7A and B. The coagulation index (BCI) of the hydrogel group was significantly lower than that of the control group. Moreover, with the extension of time, the coagulation effect became more pronounced, indicating the strong hemostatic ability of hydrogel. This can be attributed to the effective interaction between the nucleophilic cells in the blood and the phenolic groups in hydrogel. The hemostatic property of G-*O*-$B_{0.5}$ hydrogel was further evaluated *in vivo* using mouse models of tail amputation and liver hemorrhage, as illustrated in Fig. 7C, D, and E. In the untreated (control) group, the average bleeding volumes from the tail and liver were 60.63 mg and 267.03 mg, respectively. In contrast, mice treated with G-*O*-$B_{0.5}$ hydrogel exhibited average bleeding amounts of 23.9 mg from the tail and 46.96 mg from the liver. Notably, the application of hydrogel significantly reduced blood loss in both models. These findings indicate the superior hemostatic activity of G-*O*-$B_{0.5}$ hydrogel dressing.

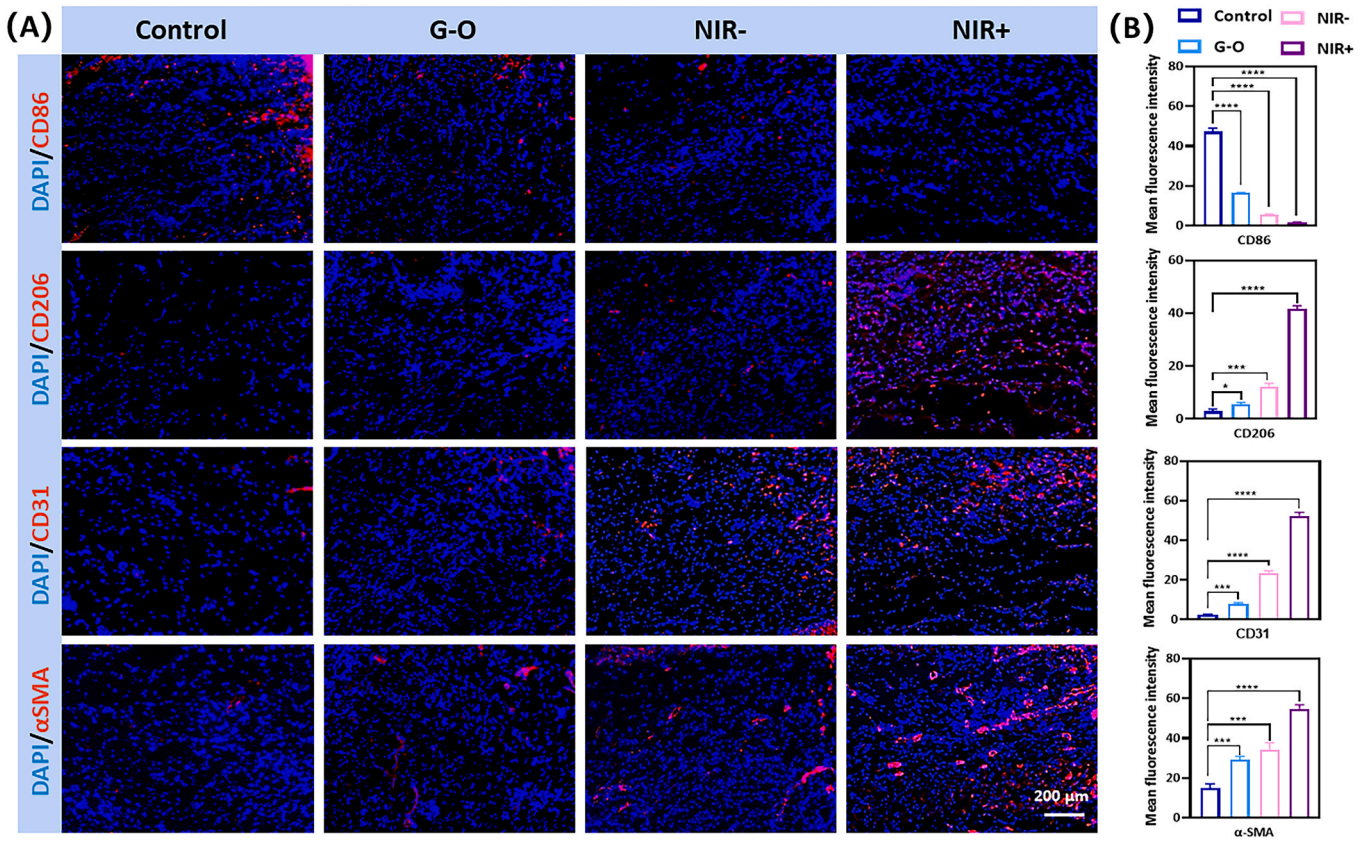

Fig. 9. (A) Immunofluorescence staining of CD86, CD206, CD31, and α-SMA to analyze wound inflammation, angiogenesis; (B) Statistical results of positive expression in each group on day 14. *p < 0.05, **p < 0.01, ***p < 0.001, ****p < 0.0001, mean ± SD, n = 3.

3.7. Wound healing of a deep secondary burn skin wound model in mice infected with Staphylococcus aureus

Burns are a common health issue that can easily become infected by pathogenic bacteria [81]. To evaluate the effectiveness of G-*O*-B hydrogel in promoting burn wound healing, a burn wound model infected with *Staphylococcus aureus* was utilized. The model construction process is illustrated in Fig. 8A and B. Initially, a circular burn wound was created on the back of a mouse using a desktop temperature-controlled burn instrument. As shown in Fig. 8C, by the naked eye, the skin of freshly burned mice was white or red and blisters compared with normal mouse skin, while the necrotic area of the burn area was black or brown over time. H&E staining of tissue sections reveals that the burn group displays a significant reduction in local residual hair follicles and sweat glands, as well as extensive damage to hair follicles (blue arrows). Additionally, the tissue displays degenerated and broken collagen fibers (red arrows) and increased levels of inflammatory factors compared to normal mouse skin.

Fig. 8E shows that after three days of treatment, the number of bacteria in the wounds of the hydrogel treated groups was significantly reduced, in which the bacteria in the NIR + group were almost completely removed. This indicates that the photothermal antibacterial effect of the hydrogel is significant and it can effectively inhibit bacterial infection.

The results obtained after 3 days of treatment in Fig. 8D and F revealed that the wound contraction rate was only around 17 % in the control group due to severe infection. The G-O group without extract showed a shrinkage of approximately 13 %. The NIR-group, which received the extract but no NIR treatment, had a further increase in the wound shrinkage rate to approximately 32 %. A significant improvement was observed in the NIR + group, which was administered blackcurrant extract and NIR treatment, achieving a remarkable wound shrinkage rate of 37 %. With increased treatment duration, wounds in each group continued to shrink. After 7 days of treatment, all groups still had mild infection, with contraction rates of 50 % in the control group and 52 % in the G-O group. In comparison, the contraction rates for the NIR- and NIR + groups were 55 % and 60 %. On the 14th day, the wounds in the NIR + group had completely contracted, while in the control group only exhibited 76 % contraction. These results indicate that G-*O*-B hydrogel accelerates wound contraction with NIR assistance, providing a promising approach for wound healing.

3.8. Histological and immunochemical analysis

Infected wounds are typically accompanied by a significant infiltration of inflammatory cells [82]. On the fourteenth day, the inflammation level was assessed based on the expression of CD86 and CD206, as shown in Fig. 9A and B. The hydrogel groups exhibited a noticeable increase in the expression of anti-inflammatory cytokine CD206 compared to the control group, while the expression of the pro-inflammatory cytokine CD86 was significantly lower in the hydrogel groups. Notably, the NIR + group had the lowest levels of pro-inflammatory cytokine and the highest levels of anti-inflammatory cytokine. This can be attributed to the antibacterial property of G-*O*-B hydrogel, which help mitigate wound infection. Moreover, when loaded with blackcurrant extract, the hydrogel demonstrates strong antibacterial property post near-infrared irradiation, effectively combating *Staphylococcus aureus* infection and maintaining an moderate inflammation level in the wound environment. Neovascularization is crucial for transporting growth factors and nutrients to the wound area, reflecting the efficiency of wound healing. The level of wound neovascularization on the fourteenth day was quantitatively assessed using the expression of CD31 and α-SMA. As depicted in Fig. 9, the hydrogel groups exhibited higher levels of CD31 and α-SMA expression compared

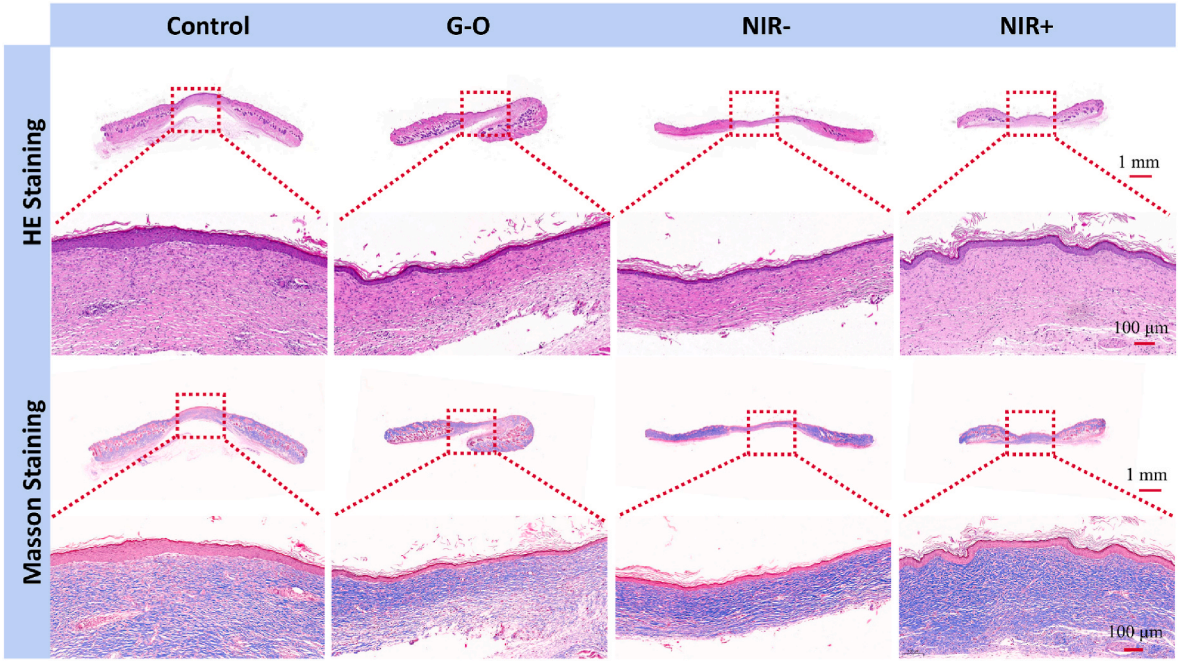

Fig. 10. H&E staining and Masson's trichrome staining of wound tissues in each group on the 14th day.

to the control group, indicating their role in promoting angiogenesis. These results support the notion that multifunctional hydrogel dressings can reduce inflammation and accelerate angiogenesis, with enhanced facilitation under NIR radiation.

Histochemical analysis using H&E staining and Masson trichrome staining is an important method to evaluate wound healing progression and the quality of regenerated skin [83]. The H&E staining images on the 14th day (Fig. 10) indicate a significant reduction in inflammation in the G-*O*-B hydrogel group, and the NIR + group exhibited a denser granulation structure in the wound area. Notably, a mature epidermis similar to normal skin was observed in the NIR + group treated with G-*O*-$B_{0.5}$ hydrogel and NIR, indicating that the combination therapy can promote the healing of infectious burn wounds. Collagen is an essential component of skin tissue, and collagen fiber content and distribution can be used to evaluate the wound healing process [84,85]. Masson staining images on the 14th day showed exciting tissue remodeling behavior in all wounds. Compared with the control group and G-O hydrogel group, the NIR + group exhibited a larger mature tissue area in the regenerated tissue with an orderly collagen network, indicating that combining G-*O*-$B_{0.5}$ hydrogel with NIR could significantly promote skin tissue regeneration. In conclusion, G-*O*-$B_{0.5}$ hydrogel can promote wound healing by inducing the formation of a compact and orderly collagen network.

4. Conclusion

In this study, a multifunctional G-*O*-B hydrogel was prepared from gelatin (G), oxidized pullulan (O), and blackcurrant extract (B) through the interaction of Schiff base reaction and hydrogen bond, and used as a new wound dressing for the repair of infected skin burn. The hydrogel shows good injectability, shape-adaptability, and biocompatibility. The introduction of B gives the hydrogel a strong antioxidant and NIR-responsive photothermal ability. The controlled photothermal temperature can realize rapid sterilization of *Staphylococcus aureus*, *Escherichia coli*, and *Pseudomonas aeruginosa*. Near-infrared assisted G-*O*-$B_{0.5}$ hydrogel can promote wound contraction and collagen deposition in a skin burn model infected with *Staphylococcus aureus*. Moreover, it was effective in regulating the level of inflammation and stimulating angiogenesis compared with the control group. Therefore, the G-*O*-$B_{0.5}$ hydrogel holds great advantages in repairing infected burn wounds.

CRediT authorship contribution statement

Yachao Yu: Writing – original draft, Methodology. **Mengyu Yang:** Methodology. **Hua Zhao:** Methodology. **Chen Zhang:** Methodology. **Kaiyue Liu:** Methodology. **Jingmei Liu:** Methodology. **Chenghao Li:** Methodology. **Bingjie Cai:** Writing – review & editing, Conceptualization. **Fangxia Guan:** Writing – review & editing, Conceptualization. **Minghao Yao:** Writing – review & editing, Validation, Conceptualization.

Declaration of competing interest

The authors declare no competing financial interest.

Data availability

Data will be made available on request.

Acknowledgements

This work was financially supported by the National Natural Science Foundation of China (U1804198) and the Key R&D and Promotion Projects in Henan Province (212102310233) from Minghao Yao, Zhongyuan Thousand Talents Project (204200510013) from Fangxia Guan. We also thank the facility support of the Center for Modern Analysis and Gene Sequencing, Zhengzhou University.

Appendix A. Supplementary data

Supplementary data to this article can be found online at https://doi.org/10.1016/j.mtbio.2024.101113.

References

[1] G. Sun, X. Zhang, Y.-I. Shen, R. Sebastian, L.E. Dickinson, K. Fox-Talbot, M. Reinblatt, C. Steenbergen, J.W. Harmon, S. Gerecht, Dextran hydrogel scaffolds enhance angiogenic responses and promote complete skin regeneration during

burn wound healing, Proc. Natl. Acad. Sci. USA 108 (52) (2011) 20976–20981, https://doi.org/10.1073/pnas.1115973108.
[2] R. Xu, G. Luo, H. Xia, W. He, J. Zhao, B. Liu, J. Tan, J. Zhou, D. Liu, Y. Wang, Z. Yao, R. Zhan, S. Yang, J. Wu, Novel bilayer wound dressing composed of silicone rubber with particular micropores enhanced wound re-epithelialization and contraction, Biomaterials 40 (2015) 1–11, https://doi.org/10.1016/j.biomaterials.2014.10.077.
[3] X. Lin, X. Yang, P. Li, Z. Xu, L. Zhao, C. Mu, D. Li, L. Ge, Antibacterial conductive collagen-based hydrogels for accelerated full-thickness wound healing, ACS Appl. Mater. Interfaces 15 (19) (2023) 22817–22829, https://doi.org/10.1021/acsami.2c22932.
[4] C. Zhou, C. Sheng, J. Chen, Y. Liang, Q. Liu, P. Li, X. Huang, B. Liu, Gradual hydrogel degradation for programable repairing full-thickness skin defect wound, Chem. Eng. J. 450 (2022) 138200, https://doi.org/10.1016/j.cej.2022.138200.
[5] X. Kang, Y. Li, Z. Duan, X. Shen, R. Fu, D. Fan, A Mxene@TA/Fe dual-nanozyme composited antifouling hydrogel for burn wound repair, Chem. Eng. J. 476 (2023) 146420, https://doi.org/10.1016/j.cej.2023.146420.
[6] X. Zhang, B. Tan, Y. Wu, M. Zhang, X. Xie, J. Liao, An injectable, self-healing carboxymethylated chitosan hydrogel with mild photothermal stimulation for wound healing, Carbohydr. Polym. 293 (2022) 119722, https://doi.org/10.1016/j.carbpol.2022.119722.
[7] S. Cheng, M. Pan, D. Hu, R. Han, L. Li, Z. Bei, Y. Li, A. Sun, Z. Qian, Adhesive chitosan-based hydrogel assisted with photothermal antibacterial property to prompt mice infected skin wound healing, Chin. Chem. Lett. 34 (12) (2023) 108276, https://doi.org/10.1016/j.cclet.2023.108276.
[8] C. Sun, W. Liu, L. Wang, R. Meng, J. Deng, R. Qing, B. Wang, S. Hao, Photopolymerized keratin-PGLa hydrogels for antibiotic resistance reversal and enhancement of infectious wound healing, Materials Today Bio 23 (2023) 100807, https://doi.org/10.1016/j.mtbio.2023.100807.
[9] Z. Geng, Z. Cao, J. Liu, Recent advances in targeted antibacterial therapy basing on nanomaterials, Exploration 3 (1) (2023), https://doi.org/10.1002/exp.20210117.
[10] N. Cortes-Penfield, M. Krsak, L. Damioli, M. Henry, J. Seidelman, A. Hewlett, L. Certain, How we approach suppressive antibiotic therapy (SAT) following debridement, antibiotics, and implant retention for prosthetic joint infection, Clin. Infect. Dis. 78 (1) (2023) 188–198, https://doi.org/10.1093/cid/ciad484.
[11] S. Abbaszadeh, M.R. Eskandari, V. Nosrati-Siahmazgi, K. Musaie, S. Mehrabi, R. Tang, M.R. Jafari, B. Xiao, V. Hosseinpour Sarmadi, F. Haghi, B.Z. Chen, X. D. Guo, H.A. Santos, M.-A. Shahbazi, A photoactive injectable antibacterial hydrogel to support chemo-immunotherapeutic effect of antigenic cell membrane and sorafenib by near-infrared light mediated tumor ablation, Materials Today Bio 19 (2023) 100609, https://doi.org/10.1016/j.mtbio.2023.100609.
[12] H. Qian, T. Lei, L. Hua, Y. Zhang, D. Wang, J. Nan, W. Liu, Y. Sun, Y. Hu, P. Lei, Fabrication, bacteriostasis and osteointegration properties researches of the additively-manufactured porous tantalum scaffolds loading vancomycin, Bioact. Mater. 24 (2023) 450–462, https://doi.org/10.1016/j.bioactmat.2022.12.013.
[13] H. Liu, F. Xing, Y. Zhou, P. Yu, J. Xu, R. Luo, Z. Xiang, P. Maria Rommens, M. Liu, U. Ritz, Nanomaterials-based photothermal therapies for antibacterial applications, Mater. Des. 233 (2023) 112231, https://doi.org/10.1016/j.matdes.2023.112231.
[14] H. Zhou, D. Tang, X. Kang, H. Yuan, Y. Yu, X. Xiong, N. Wu, F. Chen, X. Wang, H. Xiao, D. Zhou, Degradable pseudo conjugated polymer nanoparticles with NIR-II photothermal effect and cationic quaternary phosphonium structural bacteriostasis for anti-infection therapy, Adv. Sci. 9 (16) (2022) 2200732, https://doi.org/10.1002/advs.202200732.
[15] J. Li, X. Liu, L. Tan, Z. Cui, X. Yang, Y. Liang, Z. Li, S. Zhu, Y. Zheng, K.W.K. Yeung, X. Wang, S. Wu, Zinc-doped Prussian blue enhances photothermal clearance of Staphylococcus aureus and promotes tissue repair in infected wounds, Nat. Commun. 10 (1) (2019) 4490, https://doi.org/10.1038/s41467-019-12429-6.
[16] L. Liu, H. Zhang, L. Peng, D. Wang, Y. Zhang, B. Yan, J. Xie, S. Xing, F. Peng, X. Liu, A copper-metal organic framework enhances the photothermal and chemodynamic properties of polydopamine for melanoma therapy, Acta Biomater. 158 (2023) 660–672, https://doi.org/10.1016/j.actbio.2023.01.010.
[17] V.-N. Nguyen, Z. Zhao, B.Z. Tang, J. Yoon, Organic photosensitizers for antimicrobial phototherapy, Chem. Soc. Rev. 51 (9) (2022) 3324–3340, https://doi.org/10.1039/d1cs00647a.
[18] X. Wang, L. Wang, R. Fekrazad, L. Zhang, X. Jiang, G. He, X. Wen, Polyphenolic natural products as photosensitizers for antimicrobial photodynamic therapy: recent advances and future prospects, Front. Immunol. 14 (2023), https://doi.org/10.3389/fimmu.2023.1275859.
[19] X. Dai, Q. Xu, Y. Li, L. Yang, Y. Zhang, X. Liu, F. Gao, Salen-manganese complex-based nanozyme with enhanced superoxide- and catalase-like activity for wound disinfection and anti-inflammation, Chem. Eng. J. 471 (2023) 144694, https://doi.org/10.1016/j.cej.2023.144694.
[20] S.A. Eming, T. Krieg, J.M. Davidson, Inflammation in wound repair: molecular and cellular mechanisms, J. Invest. Dermatol. 127 (3) (2007) 514–525, https://doi.org/10.1038/sj.jid.5700701.
[21] Y. Tang, H. Xu, X. Wang, S. Dong, L. Guo, S. Zhang, X. Yang, C. Liu, X. Jiang, M. Kan, S. Wu, J. Zhang, C. Xu, Advances in preparation and application of antibacterial hydrogels, J. Nanobiotechnol. 21 (1) (2023) 300, https://doi.org/10.1186/s12951-023-02025-8.
[22] B. Liu, Y. Kong, O.A. Alimi, M.A. Kuss, H. Tu, W. Hu, A. Rafay, K. Vikas, W. Shi, M. Lerner, W.L. Berry, Y. Li, M.A. Carlson, B. Duan, Multifunctional microgel-based cream hydrogels for postoperative abdominal adhesion prevention, ACS Nano 17 (4) (2023) 3847–3864, https://doi.org/10.1021/acsnano.2c12104.
[23] Y. Li, Y. Han, H. Li, X. Niu, D. Zhang, K. Wang, Antimicrobial hydrogels: potential materials for medical application, Small. n/a(n/a) (2023) 2304047, https://doi.org/10.1002/smll.202304047.
[24] Y. Feng, Z. Zhang, W. Tang, Y. Dai, Gel/hydrogel-based in situ biomaterial platforms for cancer postoperative treatment and recovery, Exploration 3 (5) (2023), https://doi.org/10.1002/exp.20220173.
[25] H. Chen, D. Wu, W. Ma, C. Wu, Y. Tian, S. Wang, M. Du, Strong fish gelatin hydrogels enhanced by carrageenan and potassium sulfate, Food Hydrocolloids 119 (2021) 106841, https://doi.org/10.1016/j.foodhyd.2021.106841.
[26] Z. Aliakbar Ahovan, Z. Esmaeili, B.S. Eftekhari, S. Khosravimelal, M. Alehosseini, G. Orive, A. Dolatshahi-Pirouz, N. Pal Singh Chauhan, P.A. Janmey, A. Hashemi, S. C. Kundu, M. Gholipourmalekabadi, Antibacterial smart hydrogels: new hope for infectious wound management, Materials Today Bio 17 (2022) 100499, https://doi.org/10.1016/j.mtbio.2022.100499.
[27] L. Hu, Y. Wang, Q. Liu, M. Liu, F. Yang, C. Wang, P. Pan, L. Wang, L. Chen, J. Chen, Real-time monitoring flexible hydrogels based on dual physically cross-linked network for promoting wound healing, Chin. Chem. Lett. 34 (10) (2023) 108262, https://doi.org/10.1016/j.cclet.2023.108262.
[28] H. Ruan, M. Bek, S. Pandit, A. Aulova, J. Zhang, P. Bjellheim, M. Lovmar, I. Mijakovic, R. Kádár, Biomimetic antibacterial gelatin hydrogels with multifunctional properties for biomedical applications, ACS Appl. Mater. Interfaces 15 (47) (2023) 54249–54265, https://doi.org/10.1021/acsami.3c10477.
[29] Z. Yang, S. Chaieb, Y. Hemar, Gelatin-based nanocomposites: a review, Polym. Rev. 61 (4) (2021) 765–813, https://doi.org/10.1080/15583724.2021.1897995.
[30] R.S. Singh, N. Kaur, D. Singh, S.S. Purewal, J.F. Kennedy, Pullulan in pharmaceutical and cosmeceutical formulations: a review, Int. J. Biol. Macromol. 231 (2023) 123353, https://doi.org/10.1016/j.ijbiomac.2023.123353.
[31] S. Roy, P. Haloi, R. Choudhary, S. Chawla, M. Kumari, V.B. Konkimalla, A. Jaiswal, Quaternary pullulan-functionalized 2D MoS2 glycosheets: a potent bactericidal nanoplatform for efficient wound disinfection and healing, ACS Appl. Mater. Interfaces 15 (20) (2023) 24209–24227, https://doi.org/10.1021/acsami.3c04390.
[32] B. Xue, X. Hui, X. Chen, S. Luo, H.N.N. Dilrukshi, G. Wu, C. Chen, Application, emerging health benefits, and dosage effects of blackcurrant food formats, J. Funct. Foods 95 (2022) 105147, https://doi.org/10.1016/j.jff.2022.105147.
[33] L. Cao, Y. Park, S. Lee, D.-O. Kim, Extraction, identification, and health benefits of anthocyanins in blackcurrants (ribes nigrum L.), Appl. Sci. 11 (4) (2021), https://doi.org/10.3390/app11041863.
[34] J. Desjardins, S. Tanabe, C. Bergeron, S. Gafner, D. Grenier, Anthocyanin-rich black currant extract and cyanidin-3-O-glucoside have cytoprotective and anti-inflammatory properties, J. Med. Food 15 (12) (2012) 1045–1050, https://doi.org/10.1089/jmf.2011.0316.
[35] K.A. Kristiansen, A. Potthast, B.E. Christensen, Periodate oxidation of polysaccharides for modification of chemical and physical properties, Carbohydr. Res. 345 (10) (2010) 1264–1271, https://doi.org/10.1016/j.carres.2010.02.011.
[36] C.O. Pandeirada, M. Achterweust, H.-G. Janssen, Y. Westphal, H.A. Schols, Periodate oxidation of plant polysaccharides provides polysaccharide-specific oligosaccharides, Carbohydr. Polym. 291 (2022) 119540, https://doi.org/10.1016/j.carbpol.2022.119540.
[37] H. Amer, T. Nypelö, I. Sulaeva, M. Bacher, U. Henniges, A. Potthast, T. Rosenau, Synthesis and characterization of periodate-oxidized polysaccharides: dialdehyde xylan (DAX), Biomacromolecules 17 (9) (2016) 2972–2980, https://doi.org/10.1021/acs.biomac.6b00777.
[38] S. Guo, Y. Ren, R. Chang, Y. He, D. Zhang, F. Guan, M. Yao, Injectable self-healing adhesive chitosan hydrogel with antioxidative, antibacterial, and hemostatic activities for rapid hemostasis and skin wound healing, ACS Appl. Mater. Interfaces 14 (30) (2022) 34455–34469, https://doi.org/10.1021/acsami.2c08870.
[39] K. Liu, C. Zhang, R. Chang, Y. He, F. Guan, M. Yao, Ultra-stretchable, tissue-adhesive, shape-adaptive, self-healing, on-demand removable hydrogel dressings with multiple functions for infected wound healing in regions of high mobility, Acta Biomater. 166 (2023) 224–240, https://doi.org/10.1016/j.actbio.2023.05.025.
[40] Y. He, K. Liu, S. Guo, R. Chang, C. Zhang, F. Guan, M. Yao, Multifunctional hydrogel with reactive oxygen species scavenging and photothermal antibacterial activity accelerates infected diabetic wound healing, Acta Biomater. 155 (2023) 199–217, https://doi.org/10.1016/j.actbio.2022.11.023.
[41] R. Chang, D. Zhao, C. Zhang, K. Liu, Y. He, F. Guan, M. Yao, PMN-incorporated multifunctional chitosan hydrogel for postoperative synergistic photothermal melanoma therapy and skin regeneration, Int. J. Biol. Macromol. 253 (2023) 126854, https://doi.org/10.1016/j.ijbiomac.2023.126854.
[42] Y. Ren, S. Ma, D. Zhang, S. Guo, R. Chang, Y. He, M. Yao, F. Guan, Functionalized injectable hyaluronic acid hydrogel with antioxidative and photothermal antibacterial activity for infected wound healing, Int. J. Biol. Macromol. 210 (2022) 218–232, https://doi.org/10.1016/j.ijbiomac.2022.05.024.
[43] J. Li, C. Wang, X. Han, S. Liu, X. Gao, C. Guo, X. Wu, Aramid nanofibers-reinforced rhein fibrous hydrogels as antibacterial and anti-inflammatory burn wound dressings, ACS Appl. Mater. Interfaces 14 (40) (2022) 45167–45177, https://doi.org/10.1021/acsami.2c12869.
[44] H.S. Siebe, A.S. Sardjan, S.C. Maßmann, J. Flapper, K.J. van den Berg, N.N.H. M. Eisink, A.P.M. Kentgens, B.L. Feringa, A. Kumar, W.R. Browne, Formation of substituted dioxanes in the oxidation of gum Arabic with periodate, Green Chem. 25 (10) (2023) 4058–4066, https://doi.org/10.1039/D2GC04923F.
[45] D. Bruneel, E. Schacht, Chemical modification of pullulan: 1. Periodate oxidation, Polymer 34 (12) (1993) 2628–2632, https://doi.org/10.1016/0032-3861(93)90600-F.
[46] S. Roy, M. Halder, P. Ramprasad, S. Dasgupta, Y. Singh, D. Pal, Oxidized pullulan exhibits potent antibacterial activity against S. aureus by disrupting its membrane integrity, Int. J. Biol. Macromol. 249 (2023) 126049, https://doi.org/10.1016/j.ijbiomac.2023.126049.

[47] J. Lei, X. Li, S. Wang, L. Yuan, L. Ge, D. Li, C. Mu, Facile fabrication of biocompatible gelatin-based self-healing hydrogels, ACS Appl. Polym. Mater. 1 (6) (2019) 1350–1358, https://doi.org/10.1021/acsapm.9b00143.
[48] T. Cui, Y. Sun, Y. Wu, J. Wang, Y. Ding, J. Cheng, M. Guo, Mechanical, microstructural, and rheological characterization of gelatin-dialdehyde starch hydrogels constructed by dual dynamic crosslinking, LWT 161 (2022) 113374, https://doi.org/10.1016/j.lwt.2022.113374.
[49] S.F. Hosseini, M. Rezaei, M. Zandi, F.F. Ghavi, Preparation and functional properties of fish gelatin–chitosan blend edible films, Food Chem. 136 (3) (2013) 1490–1495, https://doi.org/10.1016/j.foodchem.2012.09.081.
[50] Y. Qin, F. Xu, L. Yuan, H. Hu, X. Yao, J. Liu, Comparison of the physical and functional properties of starch/polyvinyl alcohol films containing anthocyanins and/or betacyanins, Int. J. Biol. Macromol. 163 (2020) 898–909, https://doi.org/10.1016/j.ijbiomac.2020.07.065.
[51] A. Burgos-Edwards, F. Jiménez-Aspee, C. Theoduloz, G. Schmeda-Hirschmann, Colonic fermentation of polyphenols from Chilean currants (Ribes spp.) and its effect on antioxidant capacity and metabolic syndrome-associated enzymes, Food Chem. 258 (2018) 144–155, https://doi.org/10.1016/j.foodchem.2018.03.053.
[52] J. Ma, D. Yin, Z. Sheng, J. Cheng, Z. Jia, T. Li, S. Qu, Delayed tensile instabilities of hydrogels, J. Mech. Phys. Solid. 168 (2022) 105052, https://doi.org/10.1016/j.jmps.2022.105052.
[53] K.A. Cook, E. Martinez-Lozano, R. Sheridan, E.K. Rodriguez, A. Nazarian, M. W. Grinstaff, Hydrogels for the management of second-degree burns: currently available options and future promise, Burns & Trauma 10 (2022) tkac047, https://doi.org/10.1093/burnst/tkac047.
[54] Q. Yu, H. Sun, Z. Yue, C. Yu, L. Jiang, X. Dong, M. Yao, M. Shi, L. Liang, Y. Wan, H. Zhang, F. Yao, J. Li, Zwitterionic polysaccharide-based hydrogel dressing as a stem cell carrier to accelerate burn wound healing, Adv. Healthcare Mater. 12 (7) (2023) 2202309, https://doi.org/10.1002/adhm.202202309.
[55] S. Zhou, M. Xie, J. Su, B. Cai, J. Li, K. Zhang, New insights into balancing wound healing and scarless skin repair, J. Tissue Eng. 14 (2023) 20417314231185848, https://doi.org/10.1177/20417314231185848.
[56] Z. Li, F. Zhou, Z. Li, S. Lin, L. Chen, L. Liu, Y. Chen, Hydrogel cross-linked with dynamic covalent bonding and micellization for promoting burn wound healing, ACS Appl. Mater. Interfaces 10 (30) (2018) 25194–25202, https://doi.org/10.1021/acsami.8b08165.
[57] R. Dimatteo, N.J. Darling, T. Segura, In situ forming injectable hydrogels for drug delivery and wound repair, Adv. Drug Deliv. Rev. 127 (2018) 167–184, https://doi.org/10.1016/j.addr.2018.03.007.
[58] Y. Yoshino, M. Ohtsuka, M. Kawaguchi, K. Sakai, A. Hashimoto, M. Hayashi, N. Madokoro, Y. Asano, M. Abe, T. Ishii, T. Isei, T. Ito, Y. Inoue, S. Imafuku, R. Irisawa, M. Ohtsuka, F. Ogawa, T. Kadono, T. Kawakami, R. Kukino, T. Kono, M. Kodera, M. Takahara, M. Tanioka, T. Nakanishi, Y. Nakamura, M. Hasegawa, M. Fujimoto, H. Fujiwara, T. Maekawa, K. Matsuo, O. Yamasaki, A. Le Pavoux, T. Tachibana, H. Ihn, C. The, Wound/Burn Guidelines, the wound/burn guidelines – 6: guidelines for the management of burns, J. Dermatol. 43 (9) (2016) 989–1010, https://doi.org/10.1111/1346-8138.13288.
[59] E.B. Souto, A.F. Ribeiro, M.I. Ferreira, M.C. Teixeira, A.A.M. Shimojo, J.L. Soriano, B.C. Naveros, A. Durazzo, M. Lucarini, S.B. Souto, A. Santini, New nanotechnologies for the treatment and repair of skin burns infections, Int. J. Mol. Sci. 21 (2) (2020), https://doi.org/10.3390/ijms21020393.
[60] X. Chen, M. Zhao, Q. Xie, S. Zhou, X. Zhong, J. Zheng, R. Yang, X. Du, J. Xia, Y. Liao, Click-hydrogel delivered aggregation-induced emissive nanovesicles for simultaneous remodeling and antibiosis of deep burn wounds, Aggregate (2023) e406, https://doi.org/10.1002/agt2.406, n/a(n/a).
[61] M. Rai, M. Wypij, A.P. Ingle, J. Trzcińska-Wencel, P. Golińska, Emerging trends in pullulan-based antimicrobial systems for various applications, Int. J. Mol. Sci. 22 (24) (2021) 13596, https://doi.org/10.3390/ijms222413596.
[62] B. Miladinović, M. Kostić, K. Šavikin, B. Đorđević, T. Mihajilov-Krstev, S. Živanović, D. Kitić, Chemical profile and antioxidative and antimicrobial activity of juices and extracts of 4 black currants varieties (Ribes nigrum L.), J. Food Sci. 79 (3) (2014) C301–C309, https://doi.org/10.1111/1750-3841.12364.
[63] Y. Lee, J.-Y. Lee, Blackcurrant (Ribes nigrum) extract Exerts an anti-inflammatory action by modulating macrophage phenotypes, Nutrients. 11 (5) (2019) 975,doi: org/10.3390/nu11050975.
[64] P. Raudsepp, J. Koskar, D. Anton, K. Meremäe, K. Kapp, P. Laurson, U. Bleive, H. Kaldmäe, M. Roasto, T. Püssa, Antibacterial and antioxidative properties of different parts of garden rhubarb, blackcurrant, chokeberry and blue honeysuckle, J. Sci. Food Agric. 99 (5) (2019) 2311–2320, https://doi.org/10.1002/jsfa.9429.
[65] N. Shao, J. Yao, Y. Qi, Y. Huang, Design of an anti-scald photothermal hydrogel for rapid bacteria removal and hemostasis, Chem. Eng. J. 476 (2023) 146642, https://doi.org/10.1016/j.cej.2023.146642.
[66] K.B. Beć, J. Grabska, C.W. Huck, Principles and applications of miniaturized near-infrared (NIR) spectrometers, Chem. Eur J. 27 (5) (2021) 1514–1532, https://doi.org/10.1002/chem.202002838.
[67] A. Ejaz, S. Waliat, M. Afzaal, F. Saeed, A. Ahmad, A. Din, H. Ateeq, A. Asghar, Y. A. Shah, A. Rafi, M.R. Khan, Biological activities, therapeutic potential, and pharmacological aspects of blackcurrants (Ribes nigrum L): a comprehensive review, Food Sci. Nutr. 11 (10) (2023) 5799–5817, https://doi.org/10.1002/fsn3.3592.
[68] S. Shang, K. Zhuang, J. Chen, M. Zhang, S. Jiang, W. Li, A bioactive composite hydrogel dressing that promotes healing of both acute and chronic diabetic skin wounds, Bioact. Mater. 34 (2024) 298–310, https://doi.org/10.1016/j.bioactmat.2023.12.026.
[69] C. Dai, S. Shih, A. Khachemoune, Skin substitutes for acute and chronic wound healing: an updated review, J. Dermatol. Treat. 31 (6) (2020) 639–648, https://doi.org/10.1080/09546634.2018.1530443.
[70] D. Moura, S. Rohringer, H.P. Ferreira, A.T. Pereira, C.C. Barrias, F.D. Magalhães, H. Bergmeister, I.C. Gonçalves, Long-term in vivo degradation and biocompatibility of degradable pHEMA hydrogels containing graphene oxide, Acta Biomater. 173 (2024) 351–364, https://doi.org/10.1016/j.actbio.2023.11.012.
[71] Y. Yang, K. Shi, K. Yu, F. Xing, H. Lai, Y. Zhou, P. Xiao, Degradable hydrogel adhesives with enhanced tissue adhesion, superior self-healing, cytocompatibility, and antibacterial property, Adv. Healthcare Mater. 11 (4) (2022), https://doi.org/10.1002/adhm.202101504.
[72] F. Gao, J. Li, L. Wang, D. Zhang, J. Zhang, F. Guan, M. Yao, Dual-enzymatically crosslinked hyaluronic acid hydrogel as a long-time 3D stem cell culture system, Biomed. Mater. 15 (4) (2020) 045013, https://doi.org/10.1088/1748-605X/ab712e.
[73] M.U.A. Khan, G.M. Stojanović, M.F.B. Abdullah, A. Dolatshahi-Pirouz, H.E. Marei, N. Ashammakhi, A. Hasan, Fundamental properties of smart hydrogels for tissue engineering applications: a review, Int. J. Biol. Macromol. 254 (2024) 127882, https://doi.org/10.1016/j.ijbiomac.2023.127882.
[74] X. Xue, Y. Hu, Y. Deng, J. Su, Recent advances in design of functional biocompatible hydrogels for bone tissue engineering, Adv. Funct. Mater. 31 (19) (2021) 2009432, https://doi.org/10.1002/adfm.202009432.
[75] Q. Zhou, X. Zhou, Z. Mo, Z. Zeng, Z. Wang, Z. Cai, L. Luo, Q. Ding, H. Li, S. Tang, A PEG-CMC-THB-PRTM hydrogel with antibacterial and hemostatic properties for promoting wound healing, Int. J. Biol. Macromol. 224 (2023) 370–379, https://doi.org/10.1016/j.ijbiomac.2022.10.130.
[76] A.K. Jaiswal, H. Chhabra, S. Narwane, N. Rege, J.R. Bellare, Hemostatic efficacy of nanofibrous matrix in rat liver injury model, Surg. Innovat. 24 (1) (2017) 23–28, https://doi.org/10.1177/1553350616675799.
[77] E. Rezvani Ghomi, S. Khalili, S. Nouri Khorasani, R. Esmaeely Neisiany, S. Ramakrishna, Wound dressings: current advances and future directions, J. Appl. Polym. Sci. 136 (27) (2019), https://doi.org/10.1002/app.47738.
[78] D. Chen, X. Liu, Y. Qi, X. Ma, Y. Wang, H. Song, Y. Zhao, W. Li, J. Qin, Poly(aspartic acid) based self-healing hydrogel with blood coagulation characteristic for rapid hemostasis and wound healing applications, Colloids Surf. B Biointerfaces 214 (2022) 112430, https://doi.org/10.1016/j.colsurfb.2022.112430.
[79] L. Liesenborghs, P. Verhamme, T. Vanassche, Staphylococcus aureus, master manipulator of the human hemostatic system, J. Thromb. Haemostasis 16 (3) (2018) 441–454.
[80] M. Bijak, J. Saluk, R. Szelenberger, P. Nowak, Popular naturally occurring antioxidants as potential anticoagulant drugs, Chem. Biol. Interact. 257 (2016) 35–45, https://doi.org/10.1016/j.cbi.2016.07.022.
[81] D. Dehari, D.N. Kumar, A. Chaudhuri, A. Kumar, R. Kumar, D. Kumar, S. Singh, G. Nath, A.K. Agrawal, Bacteriophage entrapped chitosan microgel for the treatment of biofilm-mediated polybacterial infection in burn wounds, Int. J. Biol. Macromol. 253 (2023) 127247, https://doi.org/10.1016/j.ijbiomac.2023.127247.
[82] G. Liu, M. Zu, L. Wang, C. Xu, J. Zhang, R.L. Reis, S.C. Kundu, B. Xiao, L. Duan, X. Yang, CaO2–Cu2O micromotors accelerate infected wound healing through antibacterial functions, hemostasis, improved cell migration, and inflammatory regulation, J. Mater. Chem. B 12 (1) (2024) 250–263, https://doi.org/10.1039/D3TB02335D.
[83] X. Fu, Y. Chen, G. Hu, J. Lv, J. Liu, M. Ma, X. Fu, A novel antibacterial hydrogel based on thiolated ovalbumin/gelatin with silver ions to promote wound healing in mice, Int. J. Biol. Macromol. 253 (2023) 127116, https://doi.org/10.1016/j.ijbiomac.2023.127116.
[84] D.M. Darvish, Collagen fibril formation in vitro: from origin to opportunities, Materials Today Bio 15 (2022) 100322, https://doi.org/10.1016/j.mtbio.2022.100322.
[85] L. Cui, J. Li, S. Guan, K. Zhang, K. Zhang, J. Li, Injectable multifunctional CMC/HA-DA hydrogel for repairing skin injury, Materials Today Bio 14 (2022) 100257, https://doi.org/10.1016/j.mtbio.2022.100257.